AFRL-RX-WP-TP-2010-4159

SIMULATED MICROSTRUCTURE-SENSITIVE EXTREME VALUE PROBABILITIES FOR HIGH CYCLE FATIGUE OF DUPLEX Ti-6Al-4V (PREPRINT)

Craig P. Przybyla

Georgia Institute of Technology
Materials Science and Engineering

David L. McDowell

Georgia Institute of Technology
George W. Woodruff School of Mechanical Engineering

APRIL 2010

AIR FORCE RESEARCH LABORATORY
MATERIALS AND MANUFACTURING DIRECTORATE
WRIGHT-PATTERSON AIR FORCE BASE, OH 45433-7750
AIR FORCE MATERIEL COMMAND
UNITED STATES AIR FORCE

REPORT DOCUMENTATION PAGE

Form Approved
OMB No. 0704-0188

1. REPORT DATE *(DD-MM-YY)*	2. REPORT TYPE	3. DATES COVERED *(From - To)*
April 2010	Journal Article Preprint	01 April 2010 – 01 April 2010

4. TITLE AND SUBTITLE
SIMULATED MICROSTRUCTURE-SENSITIVE EXTREME VALUE PROBABILITIES FOR HIGH CYCLE FATIGUE OF DUPLEX Ti-6Al-4V (PREPRINT)

5a. CONTRACT NUMBER
In-house

5b. GRANT NUMBER

5c. PROGRAM ELEMENT NUMBER
62102F

6. AUTHOR(S)
Craig P. Przybyla (Georgia Institute of Technology, Materials Science and Engineering)
David L. McDowell (Georgia Institute of Technology, George W. Woodruff School of Mechanical Engineering)

5d. PROJECT NUMBER
4347

5e. TASK NUMBER
RG

5f. WORK UNIT NUMBER
M02R3000

7. PERFORMING ORGANIZATION NAME(S) AND ADDRESS(ES)
Georgia Institute of Technology
Materials Science and Engineering
George W. Woodruff School of Mechanical Engineering
Atlanta, GA 30332

8. PERFORMING ORGANIZATION REPORT NUMBER
AFRL-RX-WP-TP-2010-4159

9. SPONSORING/MONITORING AGENCY NAME(S) AND ADDRESS(ES)
Air Force Research Laboratory
Materials and Manufacturing Directorate
Wright-Patterson Air Force Base, OH 45433-7750
Air Force Materiel Command
United States Air Force

10. SPONSORING/MONITORING AGENCY ACRONYM(S)
AFRL/RXLMN

11. SPONSORING/MONITORING AGENCY REPORT NUMBER(S)
AFRL-RX-WP-TP-2010-4159

12. DISTRIBUTION/AVAILABILITY STATEMENT
Approved for public release; distribution unlimited.

13. SUPPLEMENTARY NOTES
Journal article submitted to *Acta Materialia*. PAO Case Number: 88ABW-2010-1217; Clearance Date: 16 Mar 2010. Paper contains color. This work was funded in whole or in part by the Department of the Air Force. The U.S. Government has for itself and others acting on its behalf an unlimited, paid-up, nonexclusive, irrevocable worldwide license to use, modify, reproduce, release, perform, display, or disclose the work by or on behalf of the U.S. Government.

14. ABSTRACT
A newly developed microstructure-sensitive extreme value probabilistic framework for fatigue variability based on computational polycrystal plasticity is exercised to compare the driving forces for fatigue crack formation (nucleation and early growth) at room temperature for four different microstructure variants of duplex a Ti-6Al-4V alloy. The aforementioned probabilistic framework links certain extreme value fatigue response parameters with microstructure attributes at fatigue critical sites through use of marked correlation functions. By applying this framework to study the driving forces for fatigue crack formation in these microstructure variants of Ti-6Al-4V, these microstructures can be ranked in terms of relative high cycle fatigue (HCF) performance and the correlated microstructure attributes that have the most influence on the predicted fatigue response can be identified. Nonlocal fatigue indicator parameters (FIPs) based on the cyclic plastic strain averaged over domains on the length scale of the microstructure attributes (e.g. grains, phases) are used to estimate the driving force(s) for fatigue crack formation are estimated using these FIPs.

15. SUBJECT TERMS
high cycle fatigue, extreme value statistics, Ti-6Al-4V, microstructure, crystal plasticity

16. SECURITY CLASSIFICATION OF:			17. LIMITATION OF ABSTRACT:	18. NUMBER OF PAGES	19a. NAME OF RESPONSIBLE PERSON (Monitor)
a. REPORT	b. ABSTRACT	c. THIS PAGE			Reji John
Unclassified	Unclassified	Unclassified	SAR	54	19b. TELEPHONE NUMBER *(Include Area Code)* N/A

Standard Form 298 (Rev. 8-98)
Prescribed by ANSI Std. Z39-18

Simulated Microstructure-Sensitive Extreme Value Probabilities for High Cycle Fatigue of Duplex Ti-6Al-4V

Craig P. Przybyla[1,2,*] and David L. McDowell[2,3]

[1]Materials and Manufacturing Directorate, Air Force Research Laboratory,
Wright-Patterson AFB, Ohio
[2]Materials Science and Engineering
Georgia Institute of Technology, Atlanta, Georgia
[3]George W. Woodruff School of Mechanical Engineering
Georgia Institute of Technology, Atlanta, Georgia

*Corresponding Author: cpriz@gatech.edu

To be submitted to Acta Materialia
Version: February 24, 2010

Abstract

A newly developed microstructure-sensitive extreme value probabilistic framework for fatigue variability based on computational polycrystal plasticity is exercised to compare the driving forces for fatigue crack formation (nucleation and early growth) at room temperature for four different microstructure variants of duplex a Ti-6Al-4V alloy. The aforementioned probabilistic framework links certain extreme value fatigue response parameters with microstructure attributes at fatigue critical sites through use of marked correlation functions. By applying this framework to study the driving forces for fatigue crack formation in these microstructure variants of Ti-6Al-4V, these microstructures can be ranked in terms of relative high cycle fatigue (HCF) performance and the correlated microstructure attributes that have the most influence on the predicted fatigue response can be identified. Nonlocal fatigue indicator parameters (FIPs) based on the cyclic plastic strain averaged over domains on the length scale of the microstructure attributes (e.g. grains, phases) are used to estimate the driving force(s) for fatigue crack formation at the grain scale. By simulating multiple statistical volume elements (SVEs) using crystal plasticity constitutive relations, extreme value distributions of the predicted driving forces for fatigue crack formation are estimated using these FIPs. This strategy of using multiple SVEs contrasts with simulation based on a single representative volume element (RVE), which is often untenably large when considering extreme value responses. The simulations demonstrate that microstructures with smaller relative primary α grain sizes and lower volume fractions of the primary α grains tend to exhibit less variability and smaller magnitudes of the driving forces for fatigue crack formation. Additionally, the extreme value FIPs are predicted to most likely occur at clusters of primary α grains oriented for easy basal slip. In some cases, surrounding grains/phases with soft orientation shed load to less favorably oriented primary α grains, producing extreme value FIPs.

Keywords: high cycle fatigue, extreme value statistics, Ti-6Al-4V, microstructure, crystal plasticity

1. Introduction

Variability of the fatigue life of engineered components arises from microstructure stochasticity. This is particularly true for the processes of fatigue crack nucleation and microstructurally small crack growth in ductile metallic material systems, which are driven by localized plasticity and the accumulation of dislocations against obstacles or the development of particular dislocation structures (e.g., persistent slip bands) [1]. In high cycle fatigue (HCF) of metals for which cyclic stress amplitudes are below the macroscopic yield stress, plasticity is quite heterogeneous and localized at microstructure attributes that raise the local stresses sufficiently to induce flow [2], are favorably oriented for preferential yield, or both. Specific life limiting attributes can vary from specimen to specimen or from component to component due to the stochasticity of material microstructure. Thus, scatter in the HCF life of specimens or components depends on the extreme value probabilities of existing microstructure attributes that elevate the driving forces for fatigue crack formation, constituting size effects.

1.1 Extreme value statistics and metal fatigue

Current methods that estimate fatigue resistance as a function of the extreme value statistics of microstructure are limited to distributions of a single microstructure attribute; these methods do not consider the effect of multiple interacting microstructure attributes on the extreme value response distributions (e.g., fatigue crack formation). For example, Atkinson and Shi [3] reviewed various extreme value models that predict the fatigue resistance in clean steels based on the largest inclusions, which control fatigue crack formation in these materials. The first class of models discussed is based on the log-normal distribution (or any standard distribution that considers the entire population) of inclusion size. Accuracy of these models, however, is limited by the experimental difficulty of correctly capturing the tails of the distribution for inclusion size because of the paucity of extreme value data. The second class of models discussed by Atkinson and Shi is based on the classical extreme value Gumbel [4] distribution. For example, Beretta and Murakami [5] used classical Gumbel extreme value statistics to estimate the size of the largest inclusion based on specimen volume, which was subsequently used to estimate fatigue strength. The third class of models is based on the generalized Pareto distribution. Atkinson and Shi argue that the generalized Pareto distribution is more effective than the two previously described methods because it incorporates a limit on the maximum inclusion size, whereas the extreme value Gumbel distribution predicts a monotonically increasing inclusion size for increasing volume of material sampled. However, it is very difficult to estimate the upper bound on this type of attribute. Additionally, all three model classes do not consider how interactions between the inclusion and surrounding matrix or microstructure affect fatigue performance. Although first order approaches based on a single microstructure attribute (e.g., inclusion size) may be sufficient for some material systems or applications, the process of fatigue crack formation in many advanced engineering alloys is often complex and depends on the influence of multiple interacting microstructure attributes. In some cases, multiple interacting microstructure attributes exert influence at different material length scales.

Some recent computational work has considered effects of multiple microstructure attributes on fatigue response. Liao [6] used a Monte Carlo technique to generate microstructure instantiations with distributions of particle size, grain size, and grain orientation that have been randomly sampled from experimental data with known distributions. These multiple microstructure instantiations are then used to simulate the variation in fatigue response in 2024-T351 aluminum sheets. The response was estimated using FEA with elastic constitutive laws. Fatigue-relevant attributes, including particle size, grain size and grain orientation, were identified in each simulated instantiation and the distribution of these attributes was considered. These fatigue-relevant attributes were selected a priori based on experiments. The results of this Monte Carlo method correlated well with methods based on extreme value statistics and with the experiments. However, as with the previous methods discussed, correlations between the important microstructure attributes relative to their influence on the driving forces for fatigue crack formation were neglected because each critical attribute was considered independent of the others.

1.2 Fatigue crack formation in duplex α+β Ti-6Al-4V

In this work, the processes of fatigue crack formation will be considered in duplex α+β Ti-6Al-4V. Experimental observations for Ti-6Al-4V support the hypothesis that fatigue crack formation in this material system is not adequately described by a distribution of any single microstructure attribute. Fatigue crack formation in α+β Ti alloys has been associated with slip-dominated fatigue crack formation as early as the 1960s by Wells and Sullivan [7], who observed cracks form along slip bands in the α phase of Ti-6Al-4V. However, confusion persists regarding the fundamental mechanisms of fatigue crack formation in this material system. In short, it is not clear which specific microstructure attributes (or arrangements of attributes) is/are most important in the processes of fatigue crack formation. Relevant experiments that have investigated fatigue crack formation in α+β Ti alloys under typical cyclical loading conditions at room temperature are reviewed next.

In duplex α+β Ti alloys, the appearance of distinct facets in the primary α grains is commonly observed at sites of fatigue crack formation. In some cases, these facets are associated closely with basal planes oriented perpendicular to the uniaxial loading axis in Ti-6Al-4V [8, 9]. Bache [10] argued that crack formation on basal planes in grains that are unfavorably oriented for slip is due to shear stresses induced by dislocation pileup on the grain boundary in adjacent grains oriented for easy slip. This mechanism, originally postulated by Stroh [11], is thought to activate when a critical density of dislocations accumulate on the boundary such that the shear stresses in the adjacent grain (oriented for easy slip) are sufficient to induce slip on the hard oriented (i.e., nearly perpendicular to the loading direction) basal slip planes. Thus, under cyclic loading conditions a crack forms over many cycles in the hard oriented grain. This proposed mechanism is supported by the work of Baxter et al. [12] who observed slip on basal planes oriented nearly perpendicular to the loading axis in IMI 834.

In contrast, other studies have observed fatigue facet formation on basal planes favorably oriented for slip. Bridier et al. [13, 14] investigated fatigue crack formation in Ti-6Al-4V in both low cycle fatigue (LCF) and HCF, respectively, and observed that cracks mostly formed on basal slip planes and less frequently on prismatic slip

planes. In all cases, these basal and prismatic planes exhibited high Schmid factors; however, a bias was observed towards primary a grains with orientation of applied stress more towards the c-axis, indicating a preference for forming on planes that are somewhat less favorably oriented for basal (or prismatic) slip but with somewhat higher stress normal to the basal (or prismatic) plane. Subsurface fatigue crack formation on pyramidal planes in primary α grains in Ti-6Al-4V was also observed by Gilbert and Piehler [15] in grains oriented for hard basal slip (i.e., with c axis nearly parallel to the uniaxial loading direction); they noted that clusters of grains oriented favorable for slip on pyramidal <a+c> planes and grains oriented favorable for basal slip tend to favor fatigue crack formation. Jha and Larsen [16] observed in Ti-6246 that at moderate stress amplitudes (i.e., close to the macroscopic yield stress), facets near the location of initial fatigue crack formation were all inclined ~35-45° relative to the loading axis. In one sample, the facet near the location of initial fatigue crack formation appeared to be oriented about 35° relative to the loading direction in a grain oriented unfavorably for basal slip, suggesting the facet may have been formed by a <c+a> hard slip mechanism (i.e., pyramidal slip). In another sample, the facet near the location of initial fatigue crack formation developed on an apparent basal slip plane favorably oriented for slip. It is interesting to note that the grain unfavorably oriented for basal slip that developed the facet was surrounded by other grains more favorably oriented for easy slip (i.e., prismatic or basal slip). Additionally, the sample with the facet that formed in the grain oriented for hard basal slip failed at ~60,000 cycles; the other sample with the facet that formed in the grain oriented for easy basal slip failed at ~2,000,000 cycles. Szczepanski et al. [17] also observed fatigue facet formation in the very high cycle fatigue (VHCF) regime of Ti-6246 on or near basal or prismatic slip planes favorably oriented for slip.

The size of the primary α grains also appears to play a role in fatigue crack formation in duplex α+β Ti alloys. Mahajan and Margolin [18] noted that larger fatigue cracks more readily formed in primary α grains with longer paths for slip. Jha and Larsen [16] and also Szczepanski et al. [17] noted in Ti-6246 that the primary α grains that form facets tend to be larger than average. However, these grains were not necessarily the largest primary α grains in the population. This suggests that grain size plays a role in fatigue crack formation in this material system, but other attributes must also be considered.

The process of fatigue crack formation in α+β Ti alloys is further complicated when one considers the existence of local textured regions on the scale of hundreds of microns to several millimeters. These *microtextured* regions are understood to develop during processing from larger prior β grains. Bridier et al. [14] observed that microtextured regions in Ti-6Al-4V that favor slip activation in grains oriented for basal or prismatic slip are associated with distributed fatigue cracks, near the interface of bands of texture. Similar observations were made by Le Biavant et al. [19], who found distributed fatigue cracks in microtextured regions favorably oriented for basal or prismatic slip and no cracking in regions unfavorably oriented for prismatic and basal slip. Because microstructure conditions in these microtextured regions appear to favor crack formation, multiple cracks form in these regions that coalesce into a critical life limiting crack. Szczepanski et al. [17] also noted that accumulated slip in microtextured regions with high fractions of grains oriented favorably for basal or prismatic slip in Ti-6246 likely

enhances fatigue crack formation in the VHCF regime. Bantounas et al. [20] observed that fatigue crack formation was favored in regions with grains oriented for easy basal slip that are adjacent to grains whose c-axis are within about 15° of the uniaxial loading direction. They argued that cracks form in grains that are oriented for easy slip and then propagate most effectively along basal planes in surrounding grains oriented for hard basal slip. This also supports the previously mentioned observations of Gilbert and Piehler [15], who noted fatigue cracking in Ti-6Al-4V in clusters of grains oriented for pyramidal <a+c> slip and grains oriented for easy basal slip.

Simulations have also given insight into understanding many of these experimental observations. Hasija et al. [21] and Venkataramani et al. [22, 23], using dwell sensitive crystal plasticity models for α-Ti-6Al and Ti-6246, respectively, demonstrated that grains favorably oriented for basal slip transfer stress to nearby grains that are unfavorably oriented for basal slip through *load shedding*. Simulations by Dunne [24-26] for α-Ti-6Al showed that these types of *rogue grain combinations* can significantly increase the driving force for fatigue crack formation, particularly in dwell fatigue.

Based on these previous examples, it is apparent that several different microstructure attributes, including grain orientation/misorientation, grain size and local texture, have been identified as important relative to fatigue crack formation in α+β Ti alloys. In fact, Jha and Larsen [16] postulate a hierarchy of microstructure arrangements relative to their potency for localized accumulated plastic slip. Based on limited experiments, they suggest four possible underlying microstructure configurations in Ti-6246 whose probability of occurrence may relate to the observed variability in the overall fatigue life. A cluster of primary α grains and lamellar α+β colonies with aligned slip planes oriented for close to maximum shear or a cluster of primary α grains, each similarly oriented for basal $\langle a \rangle$ slip were observed at sites of subsurface fatigue crack formation in specimens with shorter fatigue lives. In contrast, the microstructure features described by a hard primary α grain (oriented unfavorably for basal $\langle a \rangle$ slip) surrounded by soft lamellar colonies and/or primary α grains favorably oriented for slip or primary α grains favorably oriented for basal $\langle a \rangle$ slip were observed to be associated with surface fatigue crack formation in specimens with longer fatigue lives. Likely, many more experiments would be needed to make any conclusions regarding the uniqueness of this set of critical microstructure configurations for fatigue damage formation in this material system.

This body of work indicates that the mechanisms of fatigue crack formation in these types of α+β Ti alloys are quite complex. Even in HCF, localized plastic slip is clearly linked to fatigue crack formation. Additionally, the multiplicity of competing failure modes increase fatigue variability, particularly in the HCF and VHCF regimes [27-29]. It is not likely that the single attribute extreme value approaches outlined previously will be able to capture the microstructure dependence of the fatigue crack formation and growth in these types of material systems. A new approach is needed to link extreme value distributions of interacting microstructure attributes that enables the identification and comparison of configurations of microstructure attributes that drive variability in fatigue life.

1.3 Correlated microstructure attributes and extreme value driving forces for fatigue crack formation

Recently a new probabilistic framework was introduced that uses extreme value marked correlation functions to quantify the interacting microstructure attributes that are most statistically significant relative to the measured or simulated extreme value distributions of response [30, 31]. Specifically, correlation functions describing the microstructure attributes potentially relevant to the operant mechanism of fatigue crack formation are selectively sampled in regions marked by certain extreme value response parameters (e.g. cyclic plastic strain range). These extreme value marked correlations can be compared to the same correlation functions sampled over the entire microstructure ensemble (without regard to response) to determine the particular correlated microstructure attributes that are most significant to the extreme value response. In general, this methodology can be applied to quantify important microstructure attributes that correlate with strong influence on the extreme value distributions of fatigue response. This probabilistic framework was coupled with multiple simulated material volumes to investigate orientation relationships important to fatigue crack formation in the PM Ni-base superalloy IN 100 [30, 31]. It was shown that the driving forces for fatigue crack formation were highest in clusters of grains oriented for cube slip near grains oriented for octahedral slip, which correlated well with experimental observations in the same material [32].

Simulation-based strategies for investigating the driving forces for fatigue crack formation at the scale of microstructure have greatly expanded in recent years. McDowell [33] outlined the use of plastic shear strain-based FIPs to estimate the driving forces for fatigue crack formation in metals associated with plastic ratcheting and reversed cyclic plasticity, i.e.,

$$\left(\Delta\varepsilon_{ij}^{p}\right)_{\text{ratch}} = \left(\varepsilon_{ij}^{p}\right)\Big|_{\text{end of the cycle}} - \left(\varepsilon_{ij}^{p}\right)\Big|_{\text{beginning of the cycle}} \tag{1}$$

and

$$\left(\Delta\varepsilon_{ij}^{p}\right)_{\text{cycle}} = \left(\varepsilon_{ij}^{p}\right)_{\max}\Big|_{\text{end of the cycle}} - \left(\Delta\varepsilon_{ij}^{p}\right)_{\text{ratch}}, \tag{2}$$

respectively, where ε_{ij}^{p} are components of the plastic strain tensor. Figure 1 illustrates these cases. Two such parameters are the maximum plastic shear strain range and Fatemi-Socie [34] damage parameter, i.e.,

$$P_{MRSS} = \frac{\left\langle \Delta\gamma_{\max}^{p} \right\rangle_{V}}{2} \tag{3}$$

and

$$P_{FS} = \frac{\left\langle \Delta\gamma_{\max}^{p} \right\rangle_{V}}{2}\left(1 + K\frac{\sigma_{\max}^{n}}{\sigma_{y}}\right) \tag{4}$$

The nonlocal maximum cyclic plastic shear strain range is computed using the ordered principal plastic strain ranges over a cycle, $\left(\Delta\varepsilon_{i}^{p}\right)_{cyc}$ for $i = 1,2,3$, as $\left\langle \Delta\gamma_{\max}^{p} \right\rangle_{V} = \left|\left[\left\langle \left(\Delta\varepsilon_{1}^{p}\right)_{cyc} \right\rangle_{V} - \left\langle \left(\Delta\varepsilon_{3}^{p}\right)_{cyc} \right\rangle_{V}\right] \Big/ 2\right|$ where $\langle * \rangle_{V}$ is

employed to denote averaging of a quantity "*" over a characteristic volume, V. Note that averaging is performed on each component of the plastic strain tensor, i.e. $\left\langle \varepsilon_{ij}^{p} \right\rangle_{V} = (1/V)\int_{V} \varepsilon_{ij}^{p} dV$. The peak stress normal to the plane of $\left\langle \Delta\gamma_{\max}^{p} \right\rangle_{V}$ is given by $\sigma_{\max}^{n}$, σ_{y} is macroscopic cyclic yield strength, and K controls the effect of the normal stress on fatigue crack formation. Here a value of $K=1$ is used based on previous studies (e.g., [31]), and is subject to refinement. Averaged over scales pertinent to the microstructure attributes relevant to the processes of fatigue crack formation, these types of FIPs have been used to investigate the relative fatigue crack formation potency of several different microstructure attributes. In martensitic gear steels, Prasannavenkatesan et al. [35] used these two parameters to characterize the relative potency of different kinds of inclusions to form grain/inclusion scale HCF cracks. Similar FIPs have also been used to characterize the influence of microstructure on fatigue crack formation in structural steel [36, 37] and Ni-base superalloys [25, 30, 31, 38, 39]. These efforts have demonstrated the utility in using these types of parameters coupled with crystal plasticity simulations to correlate microstructure scale slip with fatigue crack formation at the scale of individual grains or attributes that control slip intensification (e.g., inclusions). Although not pursuant to the present work, It is possible to confer grain scale-specific Coffin-Manson type laws for crack formation, e.g., $P_{FS} = \tilde{\gamma}_{f}' \left(N_{inc} \right)^{c}$, where $\tilde{\gamma}_{f}'$ is a rescaled fatigue ductility coefficient and c is the fatigue ductility exponent.

In this work, the same microstructure-sensitive extreme value probabilistic framework is used that was demonstrated previously for IN 100 [30, 31] to investigate the influence of the microstructure on the driving forces for fatigue crack formation in duplex Ti-6Al-4V. A similar strategy of simulating multiple statistical volume elements (SVEs) sampled from the same distributions of microstructure is used to characterize the extreme value distributions of FIPs. Extreme value marked correlation functions are sampled selectively at the locations of extreme value response (i.e., hot spots). These statistical volume elements are simulated via the finite element method using a rate sensitive crystal plasticity model calibrated to experimental measurements.

2. Methodology

2.1 Extreme value marked microstructure correlation function

A brief review of the previously developed microstructure-sensitive extreme value probabilistic framework is given [30, 31]. Based on classical extreme value probability theory (cf. [4]), the probability distribution of the extreme valued response parameter α (e.g., $\alpha \equiv$ FIP) is defined as $F^{ex}(\alpha|\Omega)$ given a window (i.e., SVE) Ω. Specifically, $F^{ex}(\alpha|\Omega)$ describes the probability that the response parameter of value α is the extreme value for a sampled SVE of microstructure Ω. The extreme value marked radial correlation function is then defined as $R^{\max(\alpha)}(\beta,\beta'|r,\Omega)dr$, denoting the probability that a microstructure attribute β located coincident with the extreme value response parameter α in Ω is located within a distance of r to $r+dr$ of a second microstructure attribute β' in any direction. An extreme value marked *n*-point correlation function, extreme value marked lineal

path correlation function, extreme value marked nearest neighbor correlation function, etc. can similarly be defined [40]. This two part statistical construct describes both the extreme value response of the microstructure as represented by the response parameter α and considers the probabilities of correlated microstructure attributes, β and β', existing in the proximity of extreme values of α in a microstructure window Ω. By comparing $R^{\max(\alpha)}\left(\beta,\beta' \mid r,\Omega\right)dr$ with the correlation function for the same microstructure attributes sampled from the complete, bulk material ensemble, given by $R\left(\beta,\beta' \mid r\right)dr$, the correlated microstructure attributes most probable to exist at locations of extreme value response can be identified. Sampling is performed on a predefined size of microstructure window Ω. Changing the size of the SVE affects the number of samples required to build up the statistics of the tail of the extreme value distribution; fewer are required as SVE size increases. Moreover, the minimum size of Ω is established by relevant spatial correlations of the neighborhood of extreme value response sites. For example, nearest and second nearest neighbor grains must be sampled to capture load shedding phenomena, while much larger values are perhaps required to capture phenomena associated with microtexture. In other words, the SVE size must be suitably long compared to the short range spatial interactions at microstructure hot spots. In general, if the SVE size is too small, the extreme value distribution resulting from compiling extreme values of a set of SVEs may not relate to the low probability tail region of interest, and may provide ambiguous information.

2.2 Crystal Plasticity Modeling of Ti-6Al-4V

In aerospace applications, α+β Ti alloys are important in view of their high strength and desirable strength-to-weight ratio. These alloys exhibit favorable properties at elevated (but moderate) temperatures depending on heat treatment and thermomechanical processing. The microstructure of typical α+β Ti alloys can range from bi-modal to fully lamellar. A bi-modal microstructure is generated by applying deformation when the material is in the α+β regime (on a phase diagram) followed by recrystallization and ageing. This processing route generates a microstructure that consists of equiaxed primary α grains dispersed among regions containing transformed β grains with embedded α laths. Texture effects in these alloys are particularly pronounced due to the low symmetry of crystallographic slip and anisotropic elasticity, as well as the contrast of properties between the α and β phases. In addition, despite their greater number of available slip systems, the β regions containing α laths tend to be more resistant to slip than the primary α grains due to the presence of the α laths and, in some cases, finer α precipitates.

The particular crystal plasticity model used in this work for duplex Ti-6Al-4V was initially developed by Mayeur and McDowell [41], extended by Zhang and McDowell [42] and then Bridier et al. [43] specifically for application to the HCF loading regime for peak stresses at or below the macroscopic yield strength. In hcp primary α, there are four different families of slip systems: three $\left\langle 11\bar{2}0\right\rangle\left(0001\right)$ basal, three $\left\langle 11\bar{2}0\right\rangle\left\{10\bar{1}0\right\}$ prismatic, six

$\langle 11\bar{2}0\rangle\{10\bar{1}1\}$ first order pyramidal <a>, and twelve $\langle 11\bar{2}3\rangle\{10\bar{1}1\}$ first order pyramidal <a+c> slip systems. However, slip is dominant in the basal and prismatic slip systems due to a relatively low critical resolved shear stress compared to the other slip systems. The lamellar α+β colonies are homogenized in this model since the individual laths range in thickness from hundreds of nanometers to several microns. A crystallographic burgers orientation relation (BOR) is maintained between the secondary α and β laths defined such that $(0001)_\alpha // \{101\}_\beta$ and $\langle 0001\rangle_\alpha // \langle 111\rangle_\beta$. The 24 possible slip systems in the lamellar region include three $\langle 11\bar{2}0\rangle(0001)$ basal, three $\langle 11\bar{2}0\rangle\{10\bar{1}0\}$ prismatic, six $\langle 11\bar{2}0\rangle\{10\bar{1}1\}$ first-order pyramidal and twelve $\langle 111\rangle\{110\}$ bcc slip systems. The bcc slip systems are transformed into the hexagonal coordinate system via the BOR. Hard slip systems in these colonies are those that intersect the α/β interface. Soft deformation modes are those on which dislocations glide parallel to the α/β interface or have parallel slip planes in both the secondary α and β phases. In particular, Bridier's [43] model is formulated to favor single slip, which has been experimentally observed to dominate at low cyclic strain amplitudes. In addition, slip in the α/β colonies is more restricted.

2.3 Ellipsoidal Packing Algorithm for Generation of Digital SVEs for Ti-6Al-4V

The extreme value fatigue response in Ti-6Al-4V is characterized via the simulation of multiple SVEs to estimate $F^{ex}(\alpha|\Omega)$ and $R^{\max(\alpha)}(\beta,\beta'|r,\Omega)$. Cyclic loading response is computed using 3D digital SVEs of microstructure using the FE package ABAQUS [44] coupled with a crystal plasticity model calibrated with experiments on duplex Ti-6Al-4V, implemented in a user-material subroutine. Using multiple SVEs sampled from predefined parent distributions of key microstructure attributes (e.g. grain size distribution, phase distribution, orientation distribution, misorientation/disorientation distribution, etc.), along with 3D periodic boundary conditions, allows the simulation of microstructure dependent variation in fatigue response.

The size of the SVE for a desired response (i.e., grain scale plasticity) is selected to be large enough such that the response parameter of interest at a particular location is unaffected by statistical variations in the microstructure at a distance away on the order of the SVE size; however, the volume need not be so large that it contains the entire distribution of response for that particular response parameter. This is in contrast to a representative volume element (RVE), defined to be sufficiently large to ensure that the distribution of local response or effective response of the volume will not change by increasing the size of the RVE or its position in the bulk material. However, a RVE of reasonable size is often impractical, either being larger than laboratory specimens or involving far too intensive calculations. This is particularly true when trying to capture extreme value distributions of microstructure response. In this work, the size of the SVEs is chosen such that the local plastic deformation response on the scale of the grains is not *substantially* affected by further increasing SVE size. In addition to local variations in slip response, it is also desired that these volumes be representative (i.e., be an RVE) in terms of the overall effective (i.e., macroscopic) elastic/plastic response. In other words, it is desired that the stress-strain

response over the SVE taken from any microstructure instantiation to be representative of any other. This is the same definition of statistical volume element used in previous work [31] and very similar to the definition of SERVEs introduced by Swaminathan and Ghosh [45, 46].

To generate SVEs Ti-6Al-4V, an ellipsoidal packing based algorithm is employed to generate digital microstructure models. This method uses known distributions of the aspect ratios of grain equivalent ellipsoids fit to grains of experimentally characterized microstructures. Using grain equivalent ellipsoids instead of other space filling methods like Voronoi tessellation allows construction of more complex grain morphologies such as elongated grains common in rolled ductile metals, and facilitates more accurate reconstruction of two phase microstructures with bi-modal size distribution such as duplex Ti-6Al-4V. For example, Brahme et al. [47] used ellipsoids fit to actual grain distributions to reconstruct Al microstructures with elongated grains. The algorithm use here was developed in part based on the work of Groeber et al. who developed ellipsoidal based methods to reconstruct polycrystalline representations of IN 100 characterized from three-dimensional serial sections [48, 49].

The ellipsoidal packing based digital microstructure generation algorithm was implemented in MATLAB [50], with logic as follows:

1) An ellipsoid is generated by randomly selecting the ellipsoid aspect ratios from a predefined distribution (e.g., beta distribution).
2) The orientation of the ellipse is randomly selected based on a predefined distribution (i.e., orientation distribution function for orientation of major axes of grain equivalent ellipsoids relative to the specimen axis).
3) The ellipsoid is randomly placed in the volume. If the ellipsoid overlaps with any previously placed ellipsoid, a new random location is selected repeatedly until no overlap exists (see
4) Figure 2a.
5) Steps 1 through 4 are repeated until the jamming limit is reached and no more non-overlapping ellipsoids can be placed in the volume.
6) The ellipsoids are then allowed to grow uniformly until all the space in the microstructure volume is filled.

A two-dimensional section of a generated microstructure using this method with a bi-modal grain size distribution is shown in Figure 2b. Comparing the aspect ratios of the ellipsoids and final grains after applying uniform grain growth, the distributions of the aspect ratios of the original ellipsoids and the equivalent ellipsoids fit to the final grains were essentially the same, as shown in Figure 3. This method gives the user much more control over grain morphology than other commonly used microstructure generation algorithms like those based on the Voronoi tessellation and allows one to easily generate bi-modal grain size distributions as shown in Figures 4 and 5. Here, the tails of the distributions are captured with higher fidelity than the tails of the grain size distribution for the microstructures generated for IN 100 previously using a Voronoi tessellation based microstructure generator [31].

2.4 Simulated Microstructures

To explore the effects of varying microstructure on the distributions of FIPs, four microstructures were generated with different grain size distributions and volume fractions of primary α. The target size of the primary α grains, α+β colonies, and the target volume fraction of the primary α phase are given in Table 1. Grain size is related to grain volume according to

$$\left\langle d_{grn} \right\rangle = 0.7 \left\langle V \right\rangle^{1/3} \tag{5}$$

where $\left\langle d_{grn} \right\rangle$ and $\left\langle V \right\rangle$ are the mean (volume averaged) grain size and grain volume, respectively [51]. The assumed mean (μ) and standard deviation (σ) of the grain size for these microstructures is also given in Table 1. In Figures 4 and 5, the target log-normal and fit cumulative distribution functions are shown for the primary α grains and α+β colonies for randomly generated fine and coarse bi-modal microstructures, respectively.

2.3 Extreme Value Statistics of Fatigue in Ti-6Al-4V

This work considers how the crystallographic attributes of the microstructure (e.g., grain orientation, grain disorientation, grain size, and grain shape distributions) affect local driving forces for fatigue crack formation in HCF. As introduced previously, the maximum plastic shear strain (MPSS) and Fatemi-Socie (FS) parameters are employed. Additionally, the cumulative effective plastic strain (CEPS), $\varepsilon_{eff}^{p} = \sqrt{(2/3)\varepsilon_{ij}^{p}\varepsilon_{ij}^{p}}$, over all cycles is considered. In each microstructure, these parameters are calculated using each of three different sized averaging volumes, as defined in Table 3. The smallest averaging volume considered is slightly larger than the mean grain size of the smallest grains (i.e., the primary α grains in Microstructures A and B). By using the same sized averaging volumes to compare the response across the range of simulated microstructure, a uniform comparison can be made of the driving forces for fatigue crack formation on the scale of the averaging volume regardless of the differing distributions of grains/phases sizes.

Multiple SVEs are constructed for Ti-6Al-4V using the ellipsoidal based microstructure generator and then simulated via FEM. In all cases, these simulations are loaded with a positive mean stress. These SVEs are all dimensioned 0.400 mm along each edge of the cuboidal microstructure block and are subjected to uniaxial cyclic strain at 0.6% peak strain with zero minimum strain (R_ε = 0) at a quasistatic strain rate of 0.002s^{-1} at room temperature. Each simulation is cycled at least ten and up to twenty times to explore how shakedown affects the extreme value distributions of the FIPs. Periodic boundary conditions are applied in all directions to simulate subsurface conditions. The voxellated meshes of these generated microstructures consist of quadrilateral elements with reduced integration (type C3D8R in ABAQUS). The specific range of the number of grains is given in

Table 2 for the different microstructures considered. There are 26 elements along each edge of the SVE or 17576 elements in all. The volume of the SVE was maintained constant in this analysis across the range of

microstructures. A meshed SVE for an arbitrary instantiation of Microstructure A is given in Figure 6 with contours of the Mises strain at the peak strain 0f 0.6% after 10 cycles. The variations in the stress fields shown in Figure 6 throughout the volume are primarily due to the mismatch of the anisotropic elastic stiffness for the differently oriented grains.

3. Results and Discussion

To understand the number of cycles required to approach a condition of plastic shakedown (i.e., stabilization of cyclic plasticity at the grain scale), a single instantiation for Microstructure A was cycled 20 times using the conditions given previously. The percentage of primary α grains and α+β colonies that exhibit an effective cumulative plastic strain above a) $1.0x10^{-10}$, b) $1.0x10^{-8}$, and c) $1.0x10^{-6}$ are shown in Figure 7. Based on the shakedown period in Figure 7, it was assumed that at least 10 cycles were required before relative stability was achieved for the cyclic plastic response. Although more cycles are desirable, due to computational limitations all subsequent simulations were subjected to 10 cycles to illustrate application of the algorithms.

Next, the extreme value distributions of the various FIPs described above are considered for the four different microstructures described in Table 1. A total of 100 SVEs were instantiated for each microstructure in Table 1. The FIPs were calculated over three different averaging volumes as defined in Table 3 along with the equivalent grain size for those averaging volumes as estimated via Equation (5). A volume average FIP centered at each element in each SVE was computed for each averaging volume. The maximum volume averaged FIP for a given SVE was defined as the extreme value FIP for that instantiation. The distribution of extreme value FIPs was then constructed for each microstructure based on values from each of 100 SVEs. For the smallest averaging volume, these distributions are plotted in Figure 8 on a Gumbel probability scale [31]. The distribution appears linear on the Gumbel scale if it fits that particular distribution exactly. Using linear least squares regression, the distribution parameters for the particular distribution of interest can be estimated.

Comparing the extreme value distributions for three different FIPs does not immediately reveal any significant differences between the distributions; the same general relative trends are observed across the range of microstructures. However, the grains predicted to exhibit the extreme value response varied between the different FIPs in as many as 10% of the SVEs simulated. It is likely that CEPS is the least desirable FIP, as the cumulative effective plastic strain can evolve dramatically during initial cycles, but then changes little during subsequent cycling. Unless it can be definitively shown that directional plastic strain accumulation drives fatigue crack formation in very early cycles (unlikely in HCF), a measure of steady state cycle by cycle plastic strain reversal or accumulation is preferred. The FS FIP likely best captures the actual mechanisms of fatigue crack formation based on the previous experimental observations of the local damage processes acting in this class of materials, although CEPS has been used in the literature [24-26]. The FS parameter is better suited to capture the effect of the normal stress that appears to promote formation of fatigue cracks on basal or prismatic slip planes with slip

plane normals that tend to be closer aligned with the loading direction [43]. As shown by McDowell and Berard [52], the FS parameter reflects mixed mode growth of small fatigue cracks. For Ti-6Al-4V it is expected to be effective in reflecting combined effects of basal slip with elevated normal stress to this plane due to intergranular interactions.

As discussed in previous work [31], it is of interest to consider the mathematical character of the extreme value distributions of the FIPs as estimated from the simulated SVEs. Assuming that X is a random variable, the maximum extreme value of a sample from X of size n can be defined as

$$Y_n = \max\left(X_1, X_2, ..., X_n\right). \tag{6}$$

If it is required that Y_n is less than some value y, then all the random variables in the same sample associated with Y_n must also be less than y. The distribution function of Y_n is defined as the probability that for a sample of size n, Y_n is less than or equal to y, *i.e.*,

$$F_{Y_n}\left(y\right) \equiv P\left(Y_n \le y\right) = P\left(X_1 \le y, X_2 \le y, ..., X_n \le y\right). \tag{7}$$

For distributions of a single variable, it has been shown that there are only three types of non-degenerated distributions to which the extreme value distributions can converge for sufficiently large sample sizes [53, 54]. The three possible non-degenerated asymptotic distributions for the maximum extreme value distributions are the (i) Gumbel (Type I), (ii) Frechét (Type II), or (ii) Weibull (Type III). Mathematically, these distributions can take the respective forms [55]

$$F_{Y_n}\left(y_n\right) = \exp\left[-e^{-\alpha_n\left(y_n - u_n\right)}\right], \tag{8}$$

$$F_{Y_n}\left(y_n\right) = \exp\left[-\left(\frac{v_n}{y_n}\right)^k\right], \tag{9}$$

and

$$F_{Y_n}\left(y_n\right) = \exp\left[-\left(\frac{\omega - y_n}{\omega - w_n}\right)^k\right]. \tag{10}$$

For the Gumbel distribution, u_n is the characteristic largest value of the initial variable X and α_n is an inverse measure of dispersion of the largest value of X. The number of samples of the initial variable X in the set of distributions of X from which Y_n is sampled is n. For the Frechét distribution, v_n is the characteristic largest value of the underlying variable X and k is a shape parameter or measure of the dispersion. Finally, in the Weibull distribution, ω is the upper bound of the initial parent distribution (i.e., $F_X\left(\omega\right) = 1$), w_n is the characteristic largest value and k is the shape parameter. The desire is to characterize a dataset as belonging to one of these three types of distributions so that mathematical properties can be used to better understand the

data. Here the Type III Weibull distribution is not considered because the authors at this time are unaware of a method to quantifying an upper bound ω for the present data.

In Figure 9, the extreme value FS FIPs calculated over a cube shaped averaging volume with equivalent grain size of 0.032mm are plotted on the a) Gumbel (Type I) and b) Frechét (Type II) probability scale along with the linear fits estimated via least squares regression. The Frechét probability scale is constructed in the same manner as the Gumbel probability scale that is described in [31]. The linearized Frechét distribution is of the form $\ln\left[1/\ln\left(1/p\right)\right] = k\ln\left(y_n\right) - k\ln\left(v_n\right)$, where p is the probability. The fitting parameters for the maximum extreme value Gumbel distribution defined by Equation (8) and the Frechét distribution defined by Equation (9) are given in Tables 4 and 5. According to the calculated R^2 values from the least squares regression of the entire extreme value dataset, the distributions appear to best fit the Frechét distribution. However, upon visual inspection, it is obvious that the distributions are not linear in Figure 9b. In fact, the distributions are much more linear on the Gumbel probability scale in Figure 9a, except for the lower tails (below about 0.5 probability) which tend to have a steeper *slope* then rest of the distribution. The higher tails (0.99 probability and above) for Microstructure B and D also exhibit increased scatter and deviate significantly from the more linear portion of the distributions on the Gumbel probability scale. Here there appears to be rare cases when the volume fraction of the primary α grain is much higher (i.e., 70% as in the case of Microstructure B and D) that there are extreme value FIPs that appear to jump up significantly magnitude relative to the rest of the distribution. It could be the case that different regimes of the FIPs associate with lower and higher probabilities of the extreme value dataset In terms of microstructure interactions; this bears further examination in future work. However, in the present work it is the Gumbel distribution appears to best characterize most of the distribution with the noted exceptions.

In Figure 10, the extreme value distribution of the FS FIP determined for each of the first 10 cycles for Microstructure A is given for the FIPs calculated over a cube shaped averaging volume with equivalent grain size of 0.032mm. From Figure 10, it can be observed that most of the shakedown occurs during the first 6-7 cycles; there is little change in the distributions for cycles 8-10. Shakedown of the extreme value distributions can be quantified by comparing the parameters of the linear fits for the Gumbel distribution that are extracted as previously explained. The inverse measure of the dispersion of these distributions, α_n, changes by as much as 50% between the initial and second cycles but changes by less than 6% between the cycles 9 and 10. However, the grains predicted to exhibit the extreme value FS FIPs differed less than 3% of the time between the 1st and 10th cycles, indicating that location of the extreme value FIP in most cases can be detected in early cycles.

In Figure 11, the distributions of the volume average Fatemi-Socie (FS) FIP calculated over an averaging volume with equivalent grain size of a) 0.054mm and b) 0.076mm are shown on a Gumbel probability scale. Comparing Figures 9a and 11, there is no significant difference in the relative distributions of the extreme value FS FIPs between the different averaging volumes considered. The larger the averaging volume for the FIP calculations, the lower the overall magnitude of the extreme value FIPs tends to be. This is reasonable because larger averaging

volumes will wash out the extreme value response over a larger area. Using larger averaging volumes, however, allows one to consider the average driving forces for fatigue crack formation over a larger area. Depending on the local barriers for microstructurally small crack growth, larger averaging volumes (relative to the distance between the dominant microstructural barriers) might better indicate the locations where the critical life limiting cracks form that are large enough to avoid being arrested by these barriers.

Based on the extreme value distributions of the FIPs, Microstructure A is predicted to have the least variability in overall fatigue performance and lower maximum driving forces for fatigue crack formation. Thus, it is likely that microstructures with small primary α grain sizes and smaller volume fractions of the primary α grains will have better fatigue performance. This is directly related to the fact that most cyclic slip is occurring in the primary α grains at the applied peak strain of 0.6%. Lower volume fractions of the primary α grains exhibit less slip activity than the microstructures with higher volume fractions of primary α grains. In addition, the smaller primary α grains have smaller mean free paths for slip.

The microstructure attributes that are coincident with the grains in which the extreme value FIPs were identified are considered next. All of the volume averaged extreme value FIPs calculated over a cube shaped averaging volume with equivalent grain size of 0.032mm were identified to be centered within primary α grains. To consider the orientation of the grains predicted to exhibit the estimated extreme value response, Schmid factors were identified for the primary α HCP slip systems including the basal, prismatic, pyramidal $\langle a \rangle$, and pyramidal $\langle a+c \rangle$ slip systems. Figure 12 shows the apparent Schmid factor (calculated based only on grain orientation relative to direction of applied uniaxial stress) for each type of slip system relates to the extreme value volume averaged FS FIP for each simulation for Microstructure A. The other microstructures demonstrated similar trends. In most cases, the grains with the maximum grain averaged FIP are oriented for easy basal slip or in a softer configuration relative to the loading direction. Additionally, maximum Schmid factors are also observed for prismatic slip in a few cases for pyramidal $\langle a \rangle$ and pyramidal $\langle a+c \rangle$ slip. When the magnitude of the Schmid factor for pyramidal $\langle a \rangle$ and pyramidal $\langle a+c \rangle$ slip is high, the magnitude of the Schmid factor for prismatic slip is also fairly high. This is significant because prismatic slip is an easier slip mode than either pyramidal $\langle a \rangle$ and pyramidal $\langle a+c \rangle$ slip; therefore, prismatic slip will likely be favored even when the resolved shear stresses on both slip systems is similar.

As noted previously, the primary α grain size has been reported to play a role in the processes of fatigue crack formation. Figure 13 shows the cross correlation between the grain volume associated with the center of the volume averaged extreme value FS FIP versus the extreme value FS FIPs for Microstructure A. The volume averaged FIPs in this case are calculated over the averaging volume of 9.83×10^{-5} with equivalent grain size of 0.032mm; the mean primary α grain size for Microstructure A is 0.025mm with an approximate volume of 4.56×10^{-5} as calculated via Equation (5) (see Table 1). The grains with the extreme value FIPs tend to be larger than

the average grain size, but the largest observed FIPs do not necessarily occur in the largest grains. This is in agreement with what has been observed experimentally in Ti-6246 [16, 17].

The extreme value marked correlation functions are also constructed to consider the crystallographic attributes that most strongly influence the predicted extreme value response. As demonstrated previously [31], the microstructure dependence of the extreme value FIPs are characterized in terms of the apparent Schmid factor for the different phases considered. Specifically, Schmid factors are identified that correlate with the extreme value response using the previously introduced extreme value marked radial correlation function for the Schmid Factor (i.e., $R^{\max(\alpha)}\left(m_a^g, m_a^{g'} \mid r, \Omega\right)$). By considering the extreme value marked correlation functions for apparent Schmid factors, the probabilities of specific grain orientations and misorientations existing coincident with the observed extreme value FIPs are indirectly considered. To construct $R^{\max(\alpha)}\left(m_a^g, m_a^{g'} \mid r, \Omega\right)$, a tessellated scale of the Schmid factor in 0.05 increments was applied. As shown previously in Figure 12, grains oriented for easy basal slip were most common at locations of the estimated extreme value FIPs. Thus, to reduce the dataset to a manageable size, the correlations between the Schmid factors were considered for basal slip between 0.45 and 0.5 for the primary α phase, and Schmid factors between 0.45 and 0.5 for the same and for the other types of slip and phases, as shown in Figures 14 and 15 for Microstructure A. The correlations that occurred with the highest significance in Microstructure A are shown in Figure 14a, which plots correlations between the primary α grains oriented for easy basal slip (i.e., with a Schmid factor for basal slip between 0.45 and 0.5) and similarly oriented grains of the same phase. In Figure 15d, the correlations are plotted that occurred with the second highest probability in Microstructure A. These correlations describe the probabilities that primary α grains oriented for easy basal slip occur near α+β colonies oriented favorably for bcc slip. Note that the active bcc slip systems considered in the crystal plasticity model are aligned with certain HCP slip systems according to $\left(0001\right)_\alpha // \left\{101\right\}_\beta$ and $\left\langle 0001\right\rangle_\alpha // \left\langle 111\right\rangle_\beta$ in order to maintain the BOR. In Figures 16-18, the correlated Schmid factors are similarly plotted for the different phases that occurred with the highest probability in microstructures B, C, and D, respectively.

In all microstructures, it was found that primary α grains oriented with a Schmid factor for basal slip between 0.45 and 0.5 (easy slip) are much more likely to be found at the location of extreme value response than in the overall microstructure. This agrees with what was found by Bridier et al. [13, 14]. When considering multiple correlated microstructure attributes, it was much more probable to find a primary α grain oriented for easy basal slip near hard oriented α+β colonies with high Schmid factors for BOR-modified bcc slip in microstructures A and B or primary α grains with high Schmid factors for pyramidal $\left\langle a+c\right\rangle$ slip in microstructures B and D. The latter previously mentioned correlated orientation relationships were also identified by Gilbert and Piehler [15] and Bantounas et al. [20] in Ti-6Al-4V. Previously cited work [21-26] demonstrated that these types of hard-soft grain combinations can dramatically increase the local stress state which in turn promotes increased plasticity in these regions. It is not surprising that simulations from microstructures A and C predict these hard-soft grain correlations

to occur with highest probability when the primary α grains oriented for easy slip are near the hard oriented α+β colonies when the volume fraction of the primary α grains is low. In microstructures B and D, the hard-soft correlations that occurred with the highest probably were observed to be between the primary α grains oriented for slip near the hard oriented primary α grains, which is expected when the volume fraction of the primary α grains is high (i.e., ~70%). Other hard-soft grain relationships in microstructure are also predicted to occur with significantly higher probabilities at sites of extreme value response than in the overall microstructure. For brevity only those in Microstructure A are shown in Figures 14c) and 14d), which describe correlations between primary α grains oriented for easy basal slip near other primary α grains oriented for harder pyramidal $\langle a \rangle$ or pyramidal $\langle a+c \rangle$ slip modes, respectively. Figure 15 shows correlations between primary α grains oriented for easy basal slip and α+β colonies that in all cases exhibit harder slip modes. In short, the same key correlated microstructure attributes (in this case grains/phases with a specific Schmid factor) were identified across the range of all the microstructures. The only significant differences among the different microstructures between the key correlated attributes identified by the extreme value marked correlations functions were the magnitudes of the probabilities that these correlated attributes exist in the regions marked by the extreme value behavior compared to the overall microstructure.

The present study illustrates how this newly devised methodology can be applied to a complex alloy system. Certain limitations are recognized in terms of applicability to specific α+β Ti alloys. In all cases the generated SVEs in this study were fit to specific grain size, orientation and disorientation distributions that could be very different from certain material systems examined experimentally. For example, the grain orientation and grain disorientation distributions were assumed to be random; however, this is not very likely in a real material system. A random ODF and DDF was chosen in this study to facilitate sampling of as many different arrangements of grains as possible to better identify the most important correlated attributes related to the processes of fatigue crack formation. In textured α+β Ti alloys, some of the arrangements identified here exist with little or no probability. There is no conceptual difficulty in applying this framework to compare effects of texture intensity and multiple components of texture on fatigue response. Additionally, in the present study only subsurface material volumes were considered since 3D periodic boundary conditions were used on SVEs. Surface effects on the driving forces for fatigue crack formation have been neglected in this work. In most cases, there are competing surface and subsurface modes of fatigue crack formation.

4. Conclusions

This work has demonstrated the use of a new microstructure-sensitive extreme value probabilistic framework that links the extreme value driving forces for fatigue crack formation from polycrystal plasticity simulations conducted on duplex Ti-6Al-4V to the important correlated microstructure attributes that most influence that extreme value response. Specifically, it is concluded that:

- The ellipsoidal based microstructure generator can be a useful tool to reproduce synthetic microstructure volumes that match predefined distributions of grain size, grain orientation and grain disorientation for two-phase polycrystalline material systems.
- Multiple statistical volume elements (SVEs) can be constructed and simulated using appropriate constitutive models to estimate extreme value distributions of key response parameters.
- Cyclic plastic strain based fatigue indicator parameters calculated over nonlocal averaging volumes on the scale of the microstructure attributes relevant to the mechanisms of fatigue crack formation can be used to identify key microstructure attributes that correlate with extreme value response.
- In agreement with experiments, primary α grains oriented favorably for basal slip (with a Schmid factor for basal slip between 0.45 and 0.5) have a much higher probability of being associated with the regions of extreme value FIPs than in the overall microstructure.
- In agreement with experiments, hard-soft grain interactions between primary α grains oriented favorably for basal slip and primary α grains oriented favorably for pyramidal $\langle a+c \rangle$ or α+β colonies oriented favorably for BOR modified bcc slip correlate with increased driving forces for fatigue crack formation over a relatively wide range of α+β Ti alloy systems.

Acknowledgments

The authors would like to acknowledge the support of the NSF Center for Computational Materials Design (NSF IIP-0541678) a joint Penn State-Georgia Tech I/UCRC, for development of extreme value HCF and VHCF statistical methods informed by microstructure-sensitive computational models. In addition, Craig P. Przybyla is grateful for the financial support of the Graduate Coop Program at the Air Force Research Laboratory at Wright-Patterson Air Force Base, Dayton, Ohio. Simulations were performed using the DOD Supercomputing Resource Center. Values for the grain sizes and volume fractions used in this study were supplied by Boeing.

References

[1] S. Suresh, *Fatigue of Materials*, 2nd ed. Cambridge: Cambridge University Press, 1998.
[2] D. L. McDowell, "Basic issues in the mechanics of high cycle metal fatigue," *International Journal of Fracture*, vol. 80, pp. 103-45, 1996.
[3] H. V. Atkinson and G. Shi, "Characterization of inclusions in clean steels: a review including the statistics of extremes methods," *Progress in Materials Science*, vol. 48, pp. 457-520, 2003.
[4] E. J. Gumbel, *Statistics of Extremes*. New York: Columbia University Press, 1958.
[5] S. Beretta and Y. Murakami, "Statistical analysis of defects for fatigue strength prediction and quality control of materials," *Fatigue and Fracture of Engineering Materials and Structures*, vol. 21, pp. 1049-1065, 1998.
[6] M. Liao, "Probabilistic modeling of fatigue related microstructural parameters in aluminum alloys," *Engineering Fracture Mechanics*, vol. 76, pp. 668-680, 2009.
[7] C. H. Wells and C. P. Sullivan, "Low-cycle fatigue crack initiation in Ti-6Al-4V," *ASM Transactions Quarterly*, vol. 62, pp. 263-&, 1969.
[8] M. R. Bache and W. J. Evans, "Impact of texture on mechanical properties in an advanced titanium alloy," *Materials Science and Engineering A*, vol. 319-321, pp. 409-414, 2001.

[9] M. R. Bache, W. J. Evans, B. Suddell, and F. R. M. Herrouin, "The effects of texture in titanium alloys for engineering components under fatigue," *International Journal of Fatigue*, vol. 23, pp. S153-S159, 2001.

[10] M. R. Bache, "A review of dwell sensitive fatigue in titanium alloys: The role of microstructure, texture and operating conditions," *International Journal of Fatigue*, vol. 25, pp. 1079-1087, 2003.

[11] A. N. Stroh, "The formation of cracks as a result of plastic flow," *Proceedings of the Royal Society of London Series A*, vol. 223, pp. 404-414, 1954.

[12] G. J. Baxter, W. M. Rainforth, and L. Grabowski, "TEM observations of fatigue damage accumulation at the surface of the near-alpha titanium alloy IMI 834," *Acta Materialia*, vol. 44, pp. 3453-3463, 1996.

[13] F. Bridier, P. Villechaise, and J. Mendez, "Analyis of slip and crack initiation processes activated by fatigue in a α/β titanium alloy in relation with local crystallographic orientation," presented at 9th International Fatigue Congress, Atlanta, GA, 2006.

[14] F. Bridier, P. Villechaise, and J. Mendez, "Slip and fatigue crack formation processes in an α/β titanium alloy in relation to crystallographic texture on different scales," *Acta Materialia*, vol. 56, pp. 3951-3962, 2008.

[15] J. L. Gilbert and H. R. Piehler, "On the nature and crystallographic orientation of subsurface cracks in high cycle fatigue of Ti-6Al-4V," *Metallurgical Transactions A*, vol. 24, pp. 669-680, 1993.

[16] S. K. Jha and J. M. Larsen, "Random heterogeneity scales and probabilistic description of the long-lifetime regime of fatigue," in *Fourth International Conference on Very High Cycle Fatigue (VHCF-4)*, J. E. Allison, J. W. Jones, J. M. Larsen, and R. O. Ritchie, Eds. Ann Arbor, Michigan, USA: The Minerals, Metals and Materials Society (TMS), 2007, pp. 385-96.

[17] C. J. Szczepanski, S. K. Jha, J. M. Larsen, and J. W. Jones, "Microstructural influences on very-high-cycle fatigue-crack initiation in Ti-6246," *Metallurgical and Materials Transactions A*, vol. 39A, pp. 2841-2851, 2008.

[18] Y. Mahajan and H. Margolin, "Low-cycle fatigue behavior of Ti-6Al-2Sn-4Zr-6Mo .1. The role of microstructure in low-cycle crack nucleation and early crack-growth," *Metallurgical Transactions A*, vol. 13, pp. 257-268, 1982.

[19] K. Le Biavant, S. Pommier, and C. Prioul, "Local texturing and fatigue crack initiation in Ti-6Al-4V titanium alloy," *Fatigue and Fracture of Engineering Materials and Structures*, vol. 25, pp. 527-545, 2002.

[20] I. Bantounas, D. Dye, and T. C. Lindley, "The effect of grain orientation on fracture morphology during high-cycle fatigue of Ti-6Al-4V," *Acta Materialia*, vol. 57, pp. 3584-3595, 2009.

[21] V. Hasija, M. J. Mills, D. S. Joseph, and S. Ghosh, "Deformation and creep modeling in polycrystalline Ti-6Al alloys," *Acta Materialia*, vol. 51, pp. 4533-4549, 2003.

[22] G. Venkataramani, D. Deka, S. Ghosh, and J. B. Nordholt, "Crystal plasticity based Fe model for understanding microstructural effects on creep and dwell fatigue in Ti-6242," *Journal of Engineering Materials and Technology, Transactions of the ASME*, vol. 128, pp. 356-365, 2006.

[23] G. Venkatramani, S. Ghosh, and M. Mills, "A size-dependent crystal plasticity finite-element model for creep and load shedding in polycrystalline titanium alloys," *Acta Materialia*, vol. 55, pp. 3971-3986, 2007.

[24] F. P. E. Dunne and D. Rugg, "On the mechanisms of fatigue facet nucleation in titanium alloys," *Fatigue and Fracture of Engineering Materials and Structures*, vol. 31, pp. 949-958, 2008.

[25] F. P. E. Dunne, A. J. Wilkinson, and R. Allen, "Experimental and computational studies of low cycle fatigue crack nucleation in a polycrystal," *International Journal of Plasticity*, vol. 23, pp. 273-295, 2007.

[26] F. P. E. Dunne, D. Rugg, and A. Walker, "Lengthscale-dependent, elastically anisotropic, physically-based hcp crystal plasticity: Application to cold-dwell fatigue in Ti alloys," *International Journal of Plasticity*, vol. 23, pp. 1061-1083, 2007.

[27] S. K. Jha, J. M. Larsen, A. H. Rosenberger, and G. A. Hartman, "Dual fatigue failure modes in Ti-6Al-2Sn-4Zr-Wo and consequences on probabilistic life prediction," *Scripta Materialia*, vol. 48, pp. 1637-1642, 2003.

[28] S. K. Jha, M. J. Caton, and J. M. Larsen, "A new paradigm of fatigue variability behavior and implications for life prediction," *Materials Science and Engineering A*, vol. 468, pp. 23-32, 2007.

[29] S. K. Jha, J. M. Larsen, and A. H. Rosenberger, "Towards a physics-based description of fatigue variability behavior in probabilistic life-prediction," *Engineering Fracture Mechanics*, vol. 76, pp. 681-694, 2009.

[30] C. Przybyla, R. Prasannavenkatesan, N. Salajegheh, and D. L. McDowell, "Microstructure-sensitive modeling of high cycle fatigue," *International Journal of Fatigue*, vol. 32, pp. 512-525, 2009.

[31] C. P. Przybyla and D. L. McDowell, "Microstructure-sensitive extreme value probabilities for high cycle fatigue of Ni-base superalloy IN100," *International Journal of Plasticity*, vol. 26, pp. 372-394, 2010.
[32] K. Li, N. E. Ashbaugh, and A. H. Rosenberger, "Crystallographic Initiation of Nickel-Base Superalloy IN100 at RT and 538°C Under Low Cycle Fatigue Conditions," in *Superalloys 2004*, K. A. Green, T. M. Pollock, H. Harada, T. E. Howson, R. C. Reed, J. J. Schirra, and S. Walston, Eds. Champion, Pennsylvania: The Minerals, Metals & Materials Society (TMS), 2004.
[33] D. L. McDowell, "Simulation-based strategies for microstructure-sensitive fatigue modeling," *Materials Science and Engineering A*, vol. 468-470, pp. 4-14, 2007.
[34] A. Fatemi and D. F. Socie, "A critical plane approach to multiaxial fatigue damage including out-of-phase loading," *Fatigue and Fracture of Engineering Materials and Structures*, vol. 11, pp. 149-65, 1988.
[35] R. Prasannavenkatesan, J. X. Zhang, D. L. McDowell, G. B. Olson, and H. J. Jou, "3D modeling of subsurface fatigue crack nucleation potency of primary inclusions in heat treated and shot peened martensitic gear steels," *International Journal of Fatigue*, vol. 31, pp. 1176-1189, 2009.
[36] R. Döring, J. Hoffmeyer, T. Seeger, and M. Vormwald, "Short fatigue crack growth under nonproportional multiaxial elastic-plastic strains," *International Journal of Fatigue*, vol. 28, pp. 972-982, 2006.
[37] J. Hoffmeyer, R. Döring, T. Seeger, and M. Vormwald, "Deformation behaviour, short crack growth and fatigue lives under multiaxial nonproportional loading," *International Journal of Fatigue*, vol. 28, pp. 508-520, 2006.
[38] M. Shenoy, J. Zhang, and D. L. McDowell, "Estimating fatigue sensitivity to polycrystalline Ni-base superalloy microstructures using a computational approach," *Fatigue and Fracture of Engineering Materials and Structures*, vol. 30, pp. 889-904, 2007.
[39] K. O. Findley and A. Saxena, "Low cycle fatigue in Rene 88DT at 650 degrees C: Crack nucleation mechanisms and modeling," *Metallurgical and Materials Transactions A*, vol. 37A, pp. 1469-1475, 2006.
[40] S. Torquato, *Random heterogeneous materials : microstructure and macroscopic properties*, vol. 16. New York: Springer, 2002.
[41] J. R. Mayeur and D. L. McDowell, "A three-dimensional crystal plasticity model for duplex Ti-6Al-4V," *International Journal of Plasticity*, vol. 23, pp. 1457-1485, 2007.
[42] M. Zhang, J. Zhang, and D. L. McDowell, "Microstructure-based crystal plasticity modeling of cyclic deformation of Ti-6Al-4V," *International Journal of Plasticity*, vol. 23, pp. 1328-1348, 2007.
[43] F. Bridier, D. L. McDowell, P. Villechaise, and J. Mendez, "Crystal plasticity modeling of slip activity in Ti-6Al-4V under high cycle fatigue loading," *International Journal of Plasticity*, vol. 25, pp. 1066-1082, 2009.
[44] ABAQUS, 6.8-EF1 ed. Providence, RI, USA: Simulia, 2008.
[45] S. Swaminathan, S. Ghosh, and N. J. Pagano, "Statistically equivalent representative volume elements for unidirectional composite microstructures: Part I - Without damage," *Journal of Composite Materials*, vol. 40, pp. 583-604, 2006.
[46] S. Swaminathan and S. Ghosh, "Statistically equivalent representative volume elements for unidirectional composite microstructures: Part II - With interfacial debonding," *Journal of Composite Materials*, vol. 40, pp. 605-621, 2006.
[47] A. Brahme, M. H. Alvi, D. Saylor, J. Fridy, and A. D. Rollett, "3D reconstruction of microstructure in a commercial purity aluminum," *Scripta Materialia*, vol. 55, pp. 75-80, 2006.
[48] M. Groeber, S. Ghosh, M. D. Uchic, and D. M. Dimiduk, "A framework for automated analysis and simulation of 3D polycrystalline micro structures. Part 1: Statistical characterization," *Acta Materialia*, vol. 56, pp. 1257-1273, 2008.
[49] M. Groeber, S. Ghosh, M. D. Uchic, and D. M. Dimiduk, "A framework for automated analysis and simulation of 3D polycrystalline micro structures. Part 2: Synthetic structure generation," *Acta Materialia*, vol. 56, pp. 1274-1287, 2008.
[50] MATLAB, 7.6.0.324 (R2008a) ed: The MathWorks, Inc., 2008.
[51] V. Horalek, "ASTM Grain-size Model and Related Random Tessellation Models," *Materials Characterization*, vol. 25, pp. 263-284, 1990.
[52] D. L. McDowell and J. Y. Berard, "A ΔJ-based approach to biaxial fatigue," *Fatigue and Fracture of Engineering Materials and Structures*, vol. 15, pp. 719-41, 1992.
[53] J. Galambos, *The Asymptotic Theory of Extreme Order Statistics*. New York: John Wiley and Sons, 1978.
[54] E. Castillo, *Extreme value theory in engineering*. Boston: Academic, 1988.

[55] A. Haldar and S. Mahadevan, *Probability, Reliability and Statistical Methods in Engineering Design*. New York: John Wiley & Sons, Inc., 2000.

Tables

Table 1 Microstructures for Ti-6Al-4V along with the assumed log-normal fits for the grain volume distributions.

		Boeing Supplied Microstructures			Assumed Mean and St. Dev. for Grain Size Distributions			
					α+β Colony		Primary α	
Micro.	Name	Transformed β Size (μm)	Primary α Size (μm)	Vol % Primary α	μ (μm)	σ (μm)	μ (μm)	σ (μm)
A	Fine bi-modal low α	50	10-50	30%	50	5	25	10
B	Fine bi-modal high α	50	10-50	70%	50	5	25	10
C	Coarse bi-modal low α	80	40-60	30%	80	10	50	5
D	Coarse bi-modal high α	80	40-60	70%	80	10	50	5

Table 2 Range of number of generated grains in cubiodal SVEs dimensioned 0.400 mm along each edge for the four microstructures.

#	Name	Number of Grains
A	Fine bi-modal low α	325-375
B	Fine bi-modal high α	625-675
C	Coarse bi-modal low α	75-100
D	Coarse bi-modal high α	125-175

Table 3 Size of three different grain scale averaging volumes used to calculate FIPs. The equivalent grain size is calculated using Equation (5).

Ave. Vol.	# of Elements	Total Volume (mm^3)	Equiv. Grain Size (mm)
1	27	$9.83x10^{-5}$	0.032
2	125	$4.55x10^{-4}$	0.054
3	343	$1.25x10^{-3}$	0.076

Table 4 Fitting parameters for Microstructures A-D for the Gumbel distribution for the different averaging volumes defined in Table 3.

Ave. Vol.	Micro.	α_n	u_n	$(\alpha_n)^{-1}/u_n$	R^2
1	A	$1.257\text{x}10^{7}$	$9.387\text{x}10^{-8}$	0.85	0.98
	B	$6.562\text{x}10^{6}$	$1.117\text{x}10^{-7}$	1.36	0.79
	C	$5.032\text{x}10^{6}$	$1.008\text{x}10^{-7}$	1.97	0.93
	D	$4.968\text{x}10^{6}$	$1.485\text{x}10^{-7}$	1.36	0.88
2	A	$4.631\text{x}10^{7}$	$2.369\text{x}10^{-8}$	0.91	0.97
	B	$1.837\text{x}10^{7}$	$2.429\text{x}10^{-8}$	2.24	0.67
	C	$1.474\text{x}10^{7}$	$3.304\text{x}10^{-8}$	2.05	0.92
	D	$1.282\text{x}10^{7}$	$4.401\text{x}10^{-8}$	1.77	0.82
3	A	$1.221\text{x}10^{8}$	$9.443\text{x}10^{-9}$	0.87	0.97
	B	$4.848\text{x}10^{7}$	$1.046\text{x}10^{-8}$	1.97	0.68
	C	$3.734\text{x}10^{7}$	$1.342\text{x}10^{-8}$	2.00	0.92
	D	$3.004\text{x}10^{7}$	$1.760\text{x}10^{-8}$	1.89	0.82

Table 5 Fitting parameters for Microstructures A-D for the Frechét distribution.

Ave. Vol.	Micro.	k	v_n	R^2
1	A	1.634E+00	7.719E-08	0.91
	B	1.998E+00	1.212E-07	0.97
	C	9.570E+00	1.907E-01	0.89
	D	1.599E+00	1.378E-07	0.96

Figures

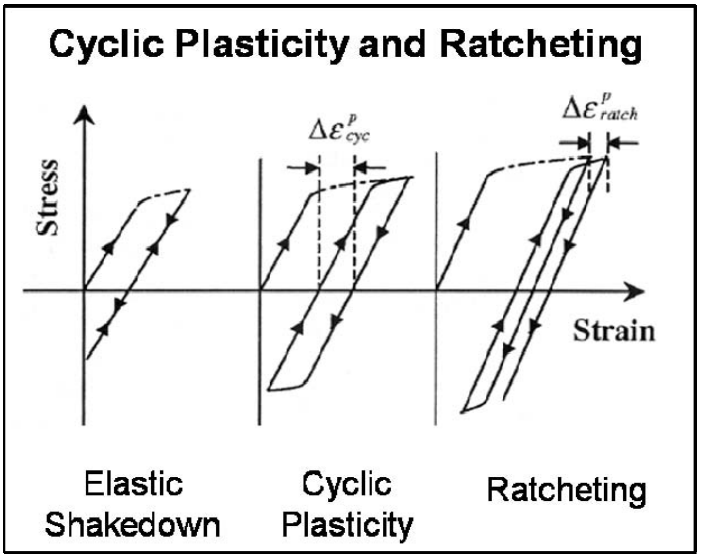

Figure 1: Schematic showing definitions of reversed cyclic plasticity $\left(\Delta\varepsilon^p\right)_{\text{cycle}}$ and ratcheting $\left(\Delta\varepsilon^p\right)_{\text{ratch}}$.

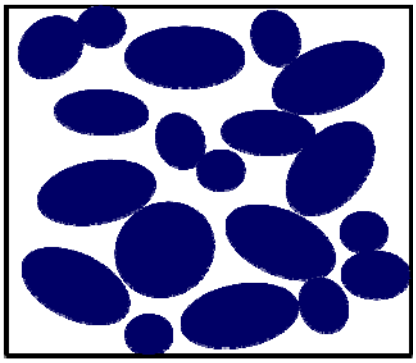

a)

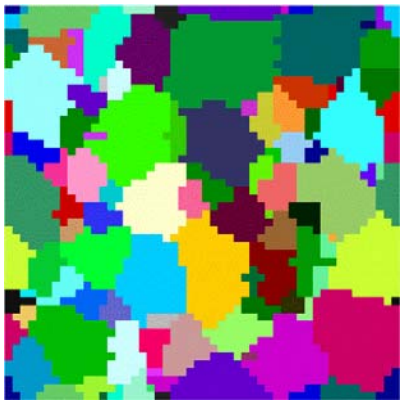

b)

Figure 2: a) A 2-D schematic demonstrating the packing of ellipses and b) a 2-D section of a microstructure generated using the ellipsoid packing algorithm with a bi-modal grain size distribution.

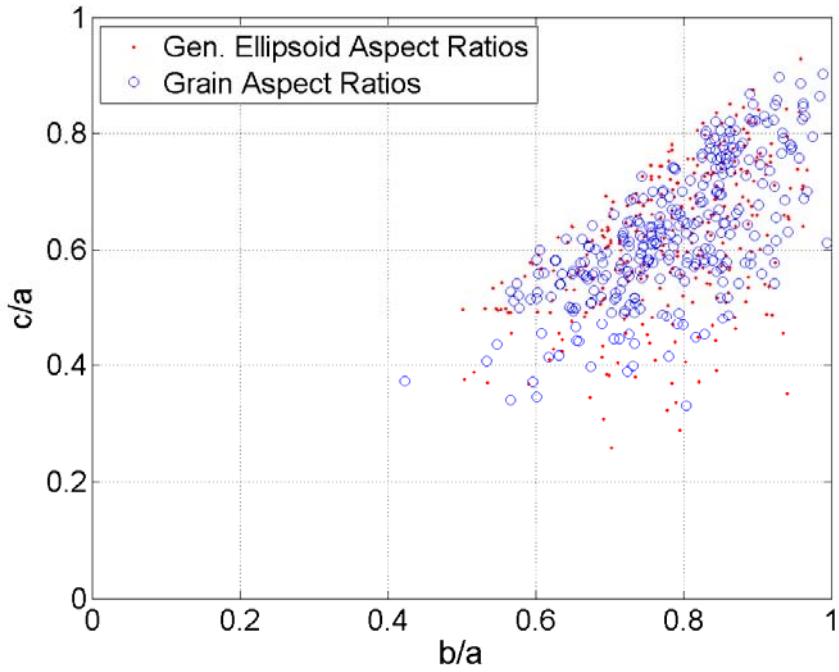

Figure 3: Aspect ratios of the initial generated ellipsoids (dots) and grains (circles) after uniform grain growth.

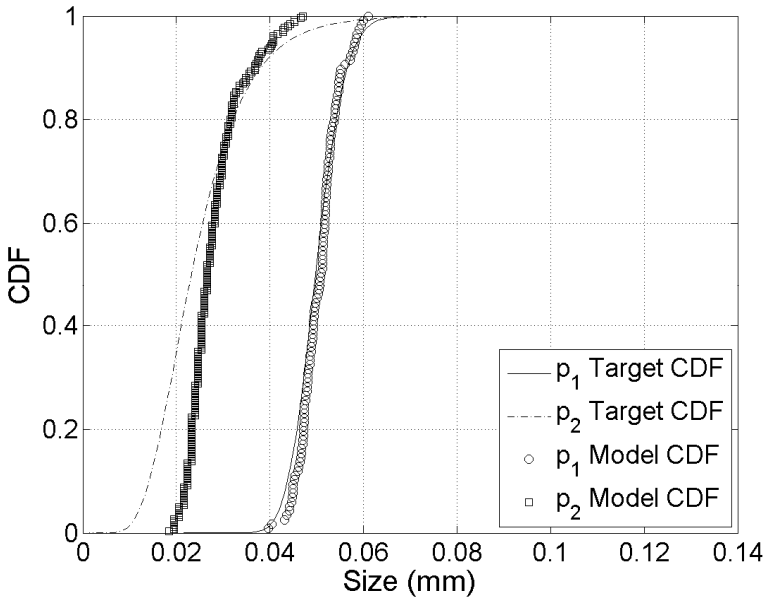

Figure 4: Target log-normal and fit model distributions of the grain size for the α+β colonies (p_1) and primary α grains (p_2) for a randomly generated fine bi-modal microstructure.

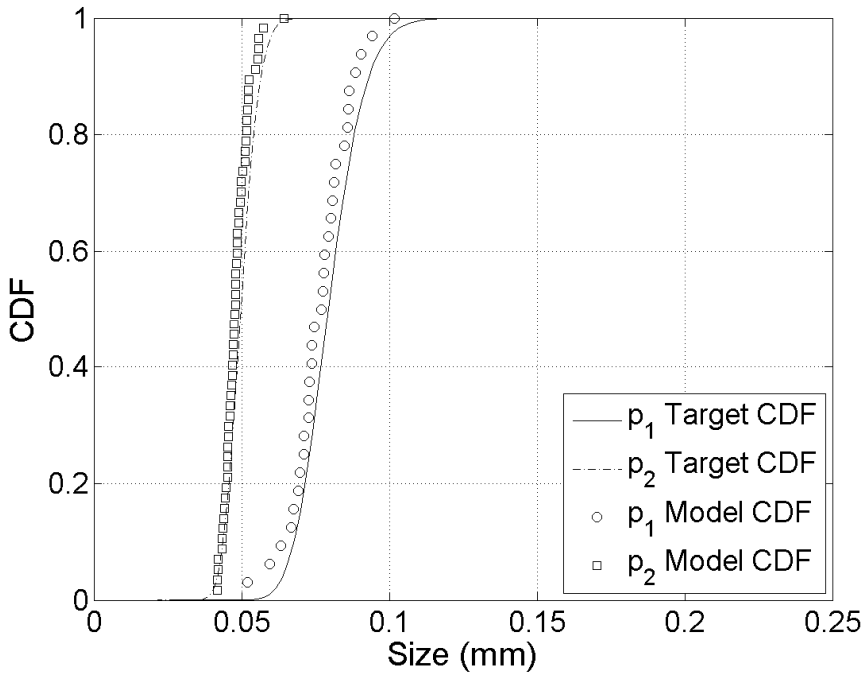

Figure 5: Target log-normal and fit model distributions of the grain size for the α+β colonies (p_1) and primary α grains (p_2) for a randomly generated coarse bi-modal microstructure.

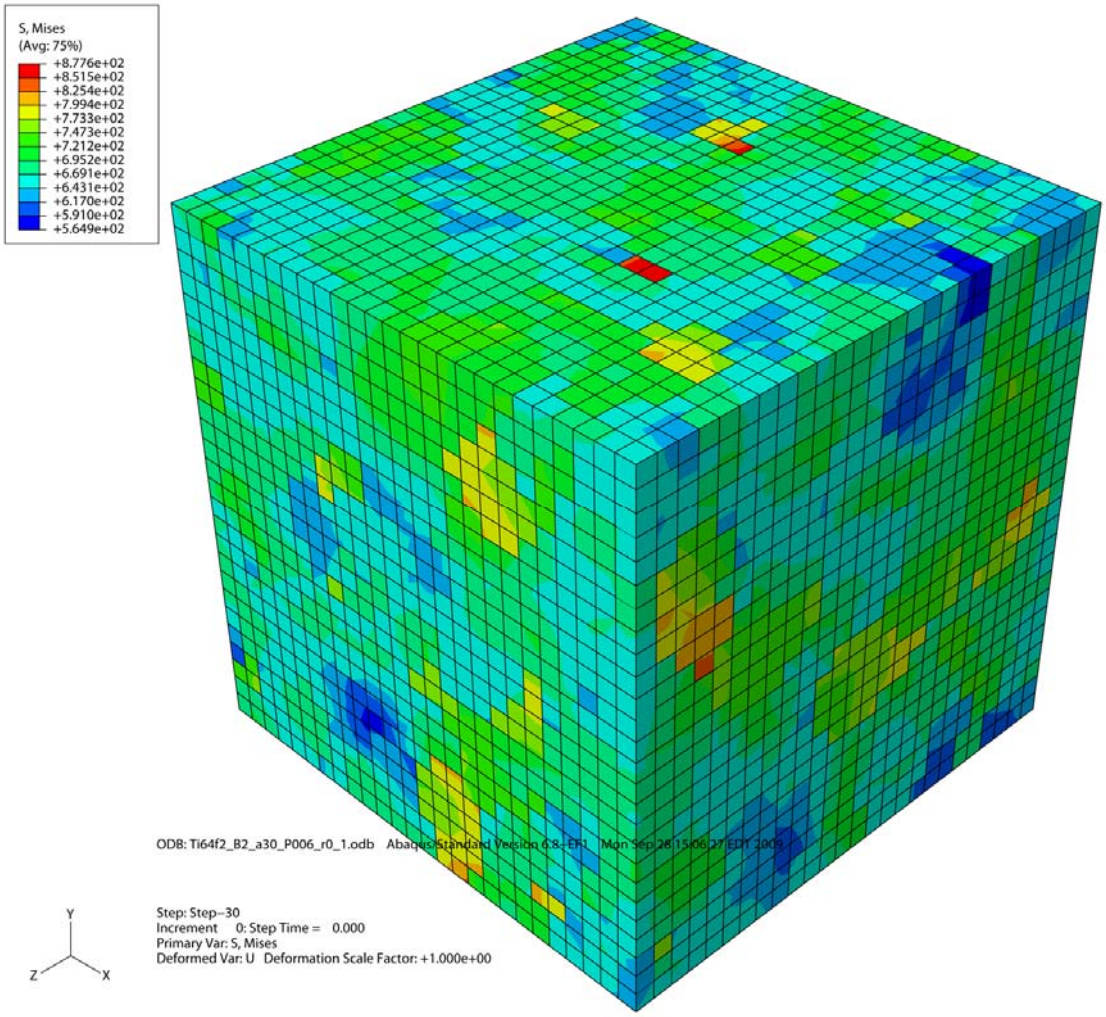

Figure 6: Meshed cuboidal SVE with an edge dimension of 0.400 mm for an arbitrary instantiation of Microstructure A with contours of the Mises stress at the peak strain of 0.6% after 10 cycles.

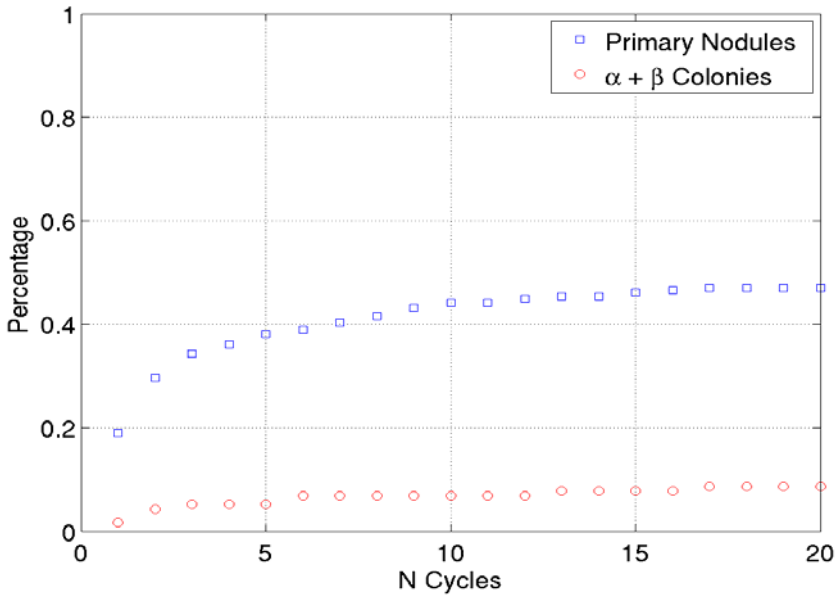
Primary Nodules
α + β Colonies
Percentage
N Cycles
0
0.2
0.4
0.6
0.8
1
0
5
10
15
20

a)

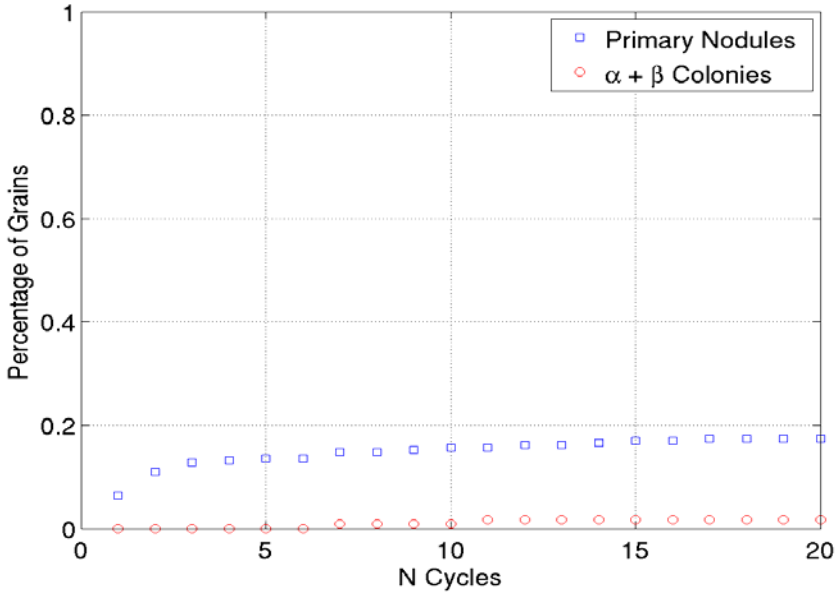
Primary Nodules
α + β Colonies
Percentage of Grains
N Cycles
0
0.2
0.4
0.6
0.8
1
0
5
10
15
20

b)

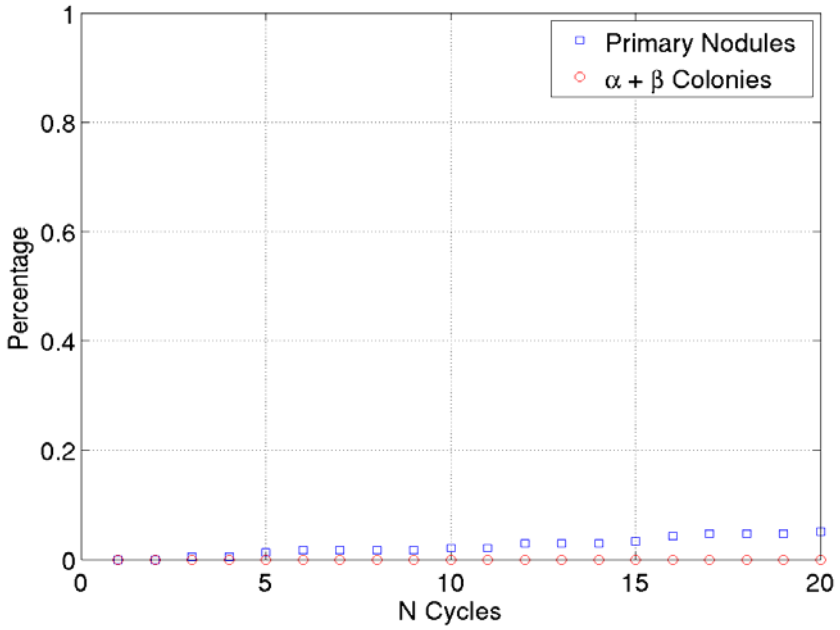

c)

Figure 7: The percentage of primary α grain and α+β colonies that exhibit an effective plastic strain above a) $1.0x10^{-10}$, b) $1.0x10^{-8}$, and c) $1.0x10^{-6}$ over for the first 20 cycles at 0.6% maximum strain for R = 0 cycling.

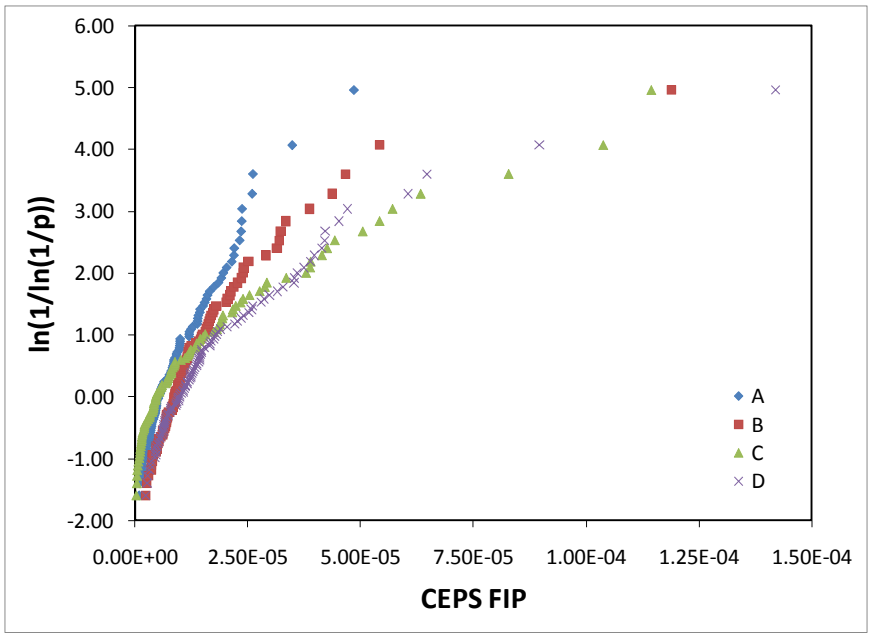
6.00
5.00
4.00
3.00
2.00
1.00
0.00
-1.00
-2.00
ln(1/ln(1/p))
0.00E+00
2.50E-05
5.00E-05
7.50E-05
1.00E-04
1.25E-04
1.50E-04
CEPS FIP
A
B
C
D

a)

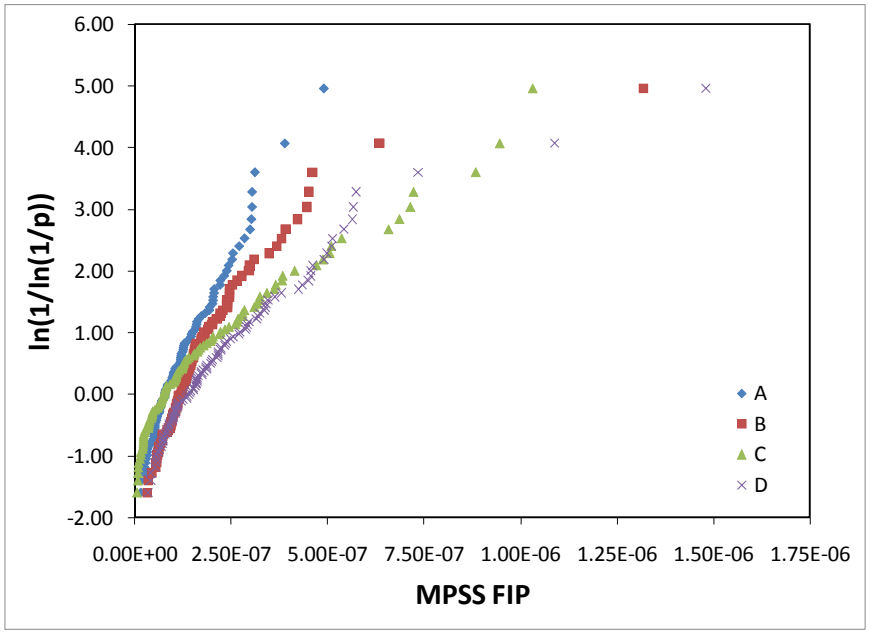
6.00
5.00
4.00
3.00
2.00
1.00
0.00
-1.00
-2.00
ln(1/ln(1/p))
0.00E+00
2.50E-07
5.00E-07
7.50E-07
1.00E-06
1.25E-06
1.50E-06
1.75E-06
MPSS FIP
A
B
C
D

b)

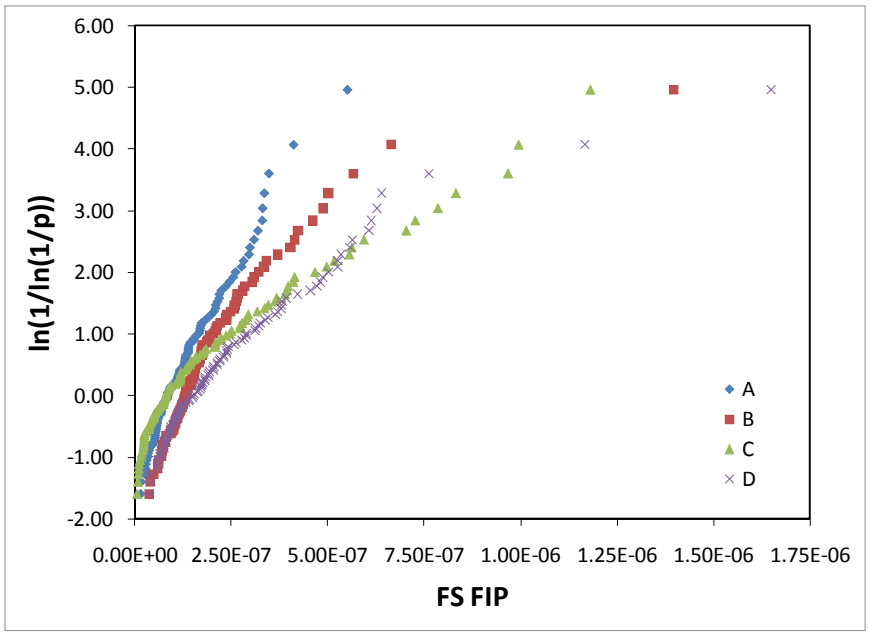

c)

Figure 8: The extreme value FIP calculated over a cube shaped averaging volume with equivalent grain size of 0.032mm for Microstructures A-D plotted on a Gumbel probability scale for a) the cumulative effective plastic strain (CEPS), b) the maximum plastic shear strain (MPSS), and c) the Fatemi-Socie (FS) FIPs.

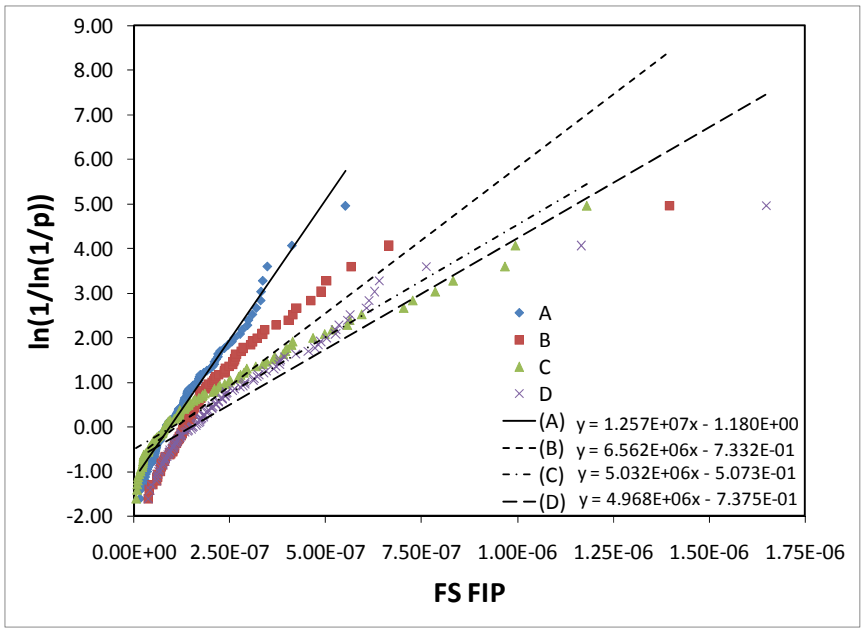

a)

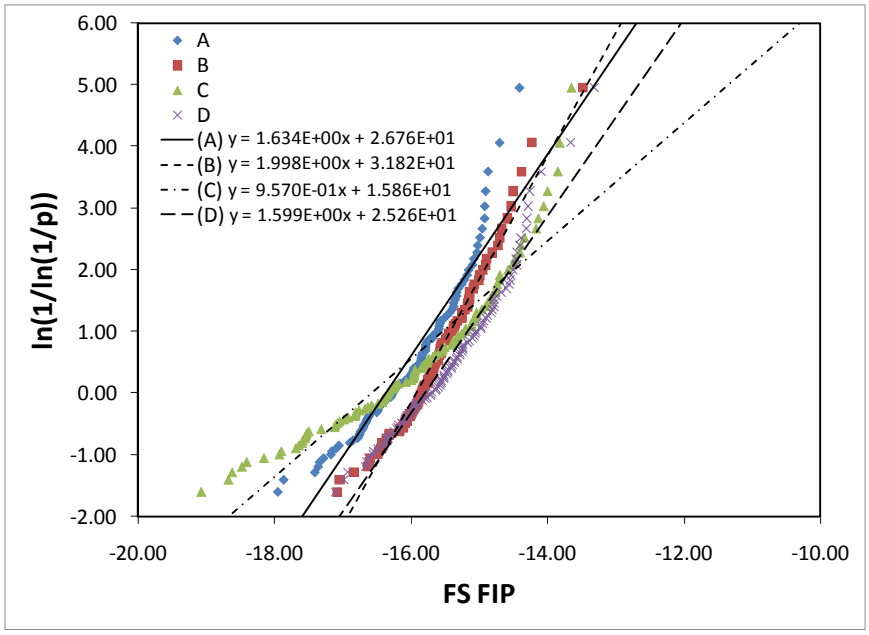

b)

Figure 9: The extreme value Fatemi-Socie (FS) FIP calculated over a cube shaped averaging volume with equivalent grain size of 0.032mm for the four analyzed microstructures plotted on a) Gumbel (Type I), b) Frechét (Type II) probability scales. Note that the equations given for the least squares linear regression are such that

$y = \ln\left(1/\ln\left(1/p\right)\right)$ and $x = \mathrm{FIP}$ for the Gumbel probability plot and $x = \ln\left(\mathrm{FIP}\right)$ for the Frechét probability plot, respectively.

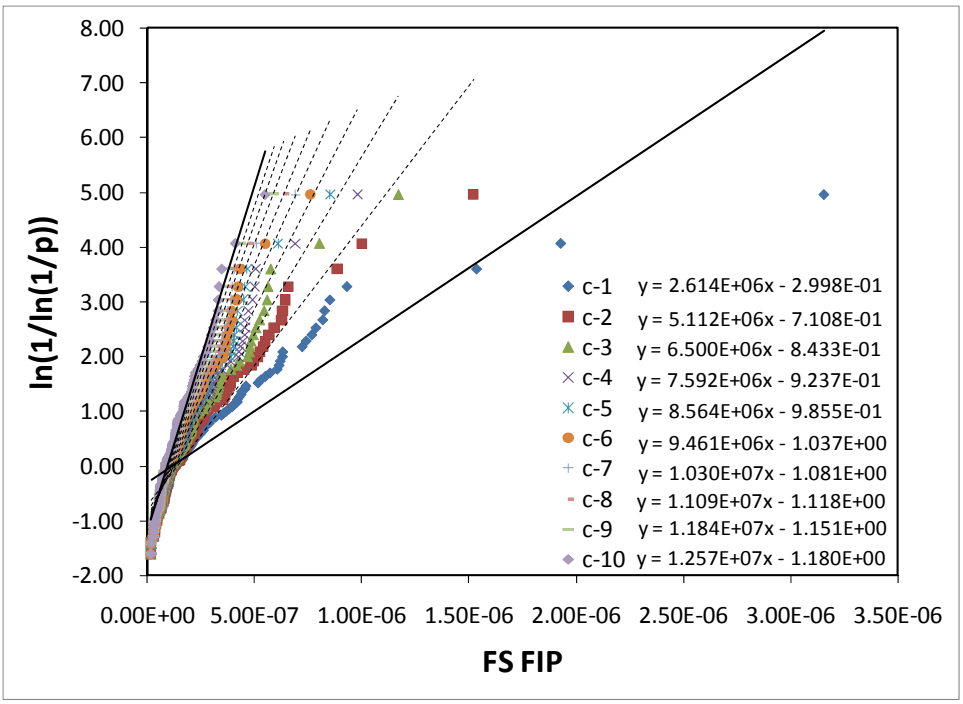

Figure 10 The extreme value Fatemi-Socie (FS) FIP calculated over a cube shaped averaging volume with equivalent grain size of 0.032mm for Microstructure A on a Gumbel probability scale for the first 10 cycles. Note that the equations given for the least squares linear regression are such that $y = \ln\left(1/\ln\left(1/p\right)\right)$ and $x = \mathrm{FIP}$.

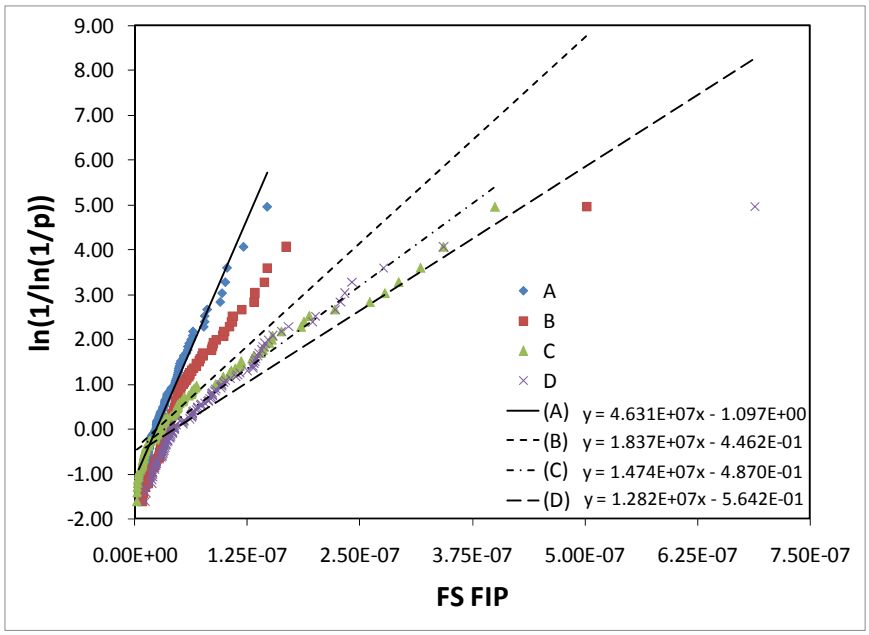

a)

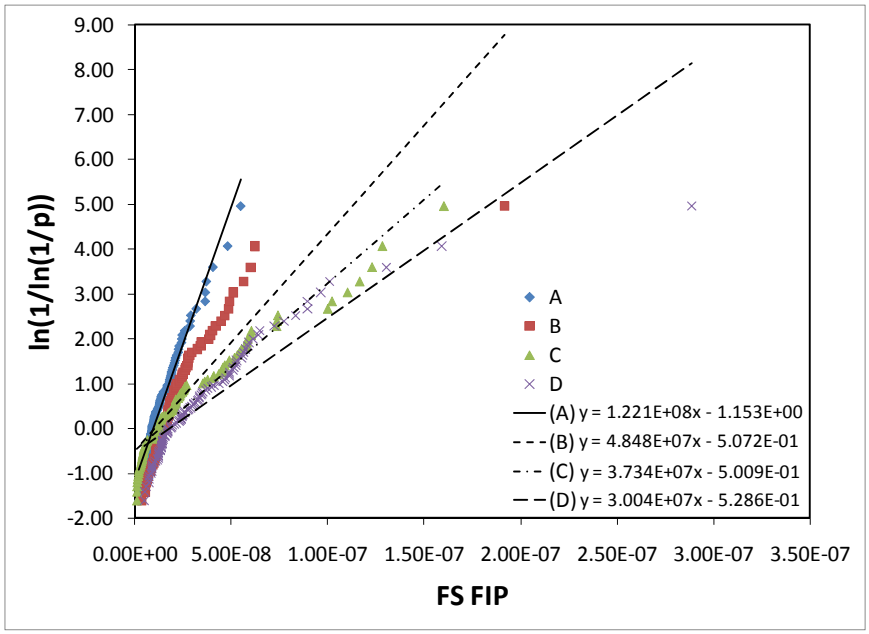

b)

Figure 11: The extreme value Fatemi-Socie (FS) FIP calculated over averaging volume with equivalent grain size of a) 0.054mm and b) 0.076mm for the range of microstructure considered on a Gumbel probability scale. Note that the equations given for the least squares linear regression are such that $y = \ln\left(1/\ln\left(1/p\right)\right)$ and $x = \mathrm{FIP}$.

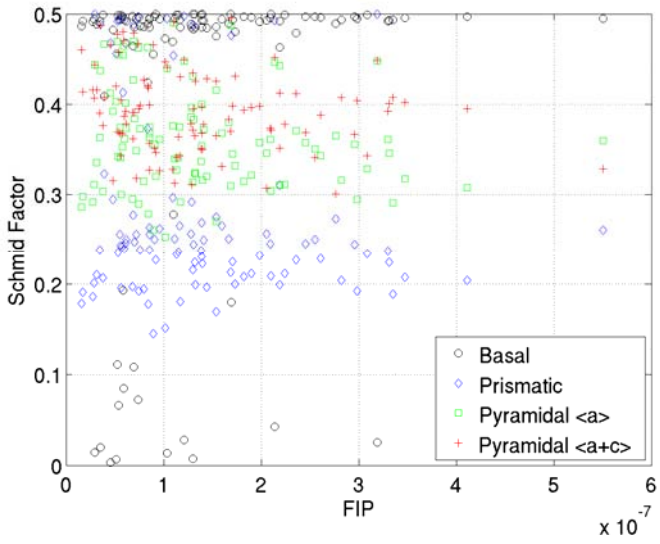

Figure 12: The Schmid factors (calculated based on the geometry of slip system relative to the loading direction) for basal, prismatic, pyramidal <a>, and pyramidal <a+c> for each extreme value Fatemi-Socie FIP calculated over a cube shaped averaging volume with equivalent grain size of 0.032mm estimated from the 100 simulated SVEs for Microstructure A.

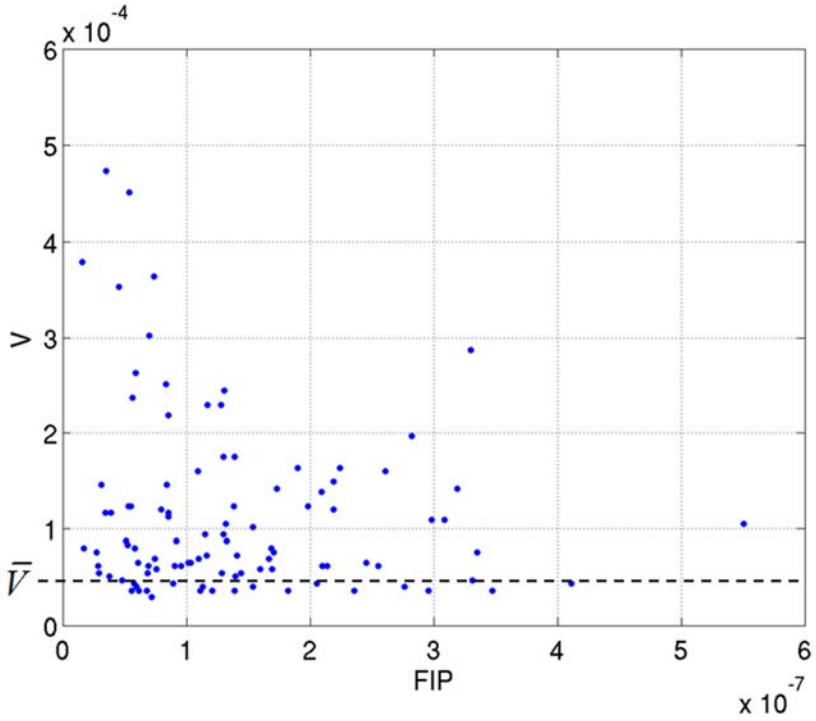

Figure 13: The extreme value Fatemi-Socie FIPs calculated over a cube shaped averaging volume with equivalent grain size of 0.032mm plotted against the grain volume of the grain coincident with the extreme value FIP for the 100 simulated SVEs for Microstructure A. The average grain volume for Microstructure A calculated via Equation (5) based on the average grain size of 0.025mm is shown by $\overline{V}$.

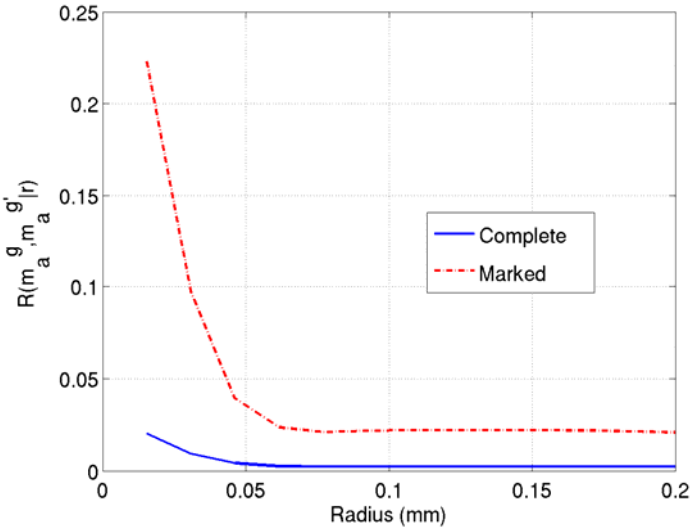
0.25
0.2
0.15
0.1
0.05
0
0
0.05
0.1
0.15
0.2
Radius (mm)
$R(m_a^g, m_a^{g'}|r)$
Complete
Marked

a)

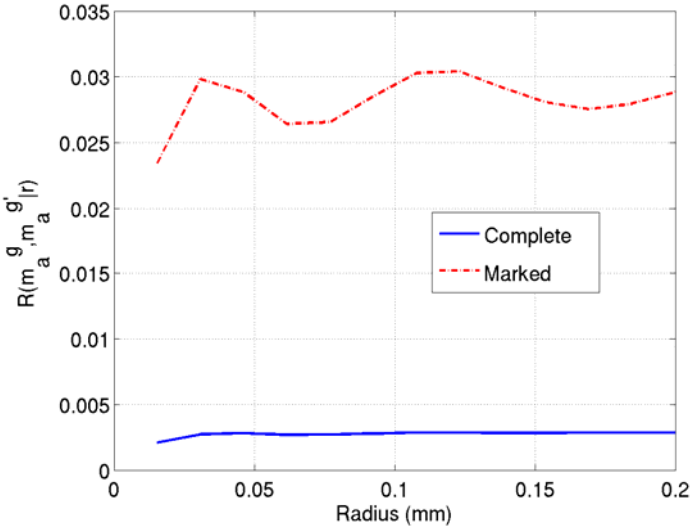
0.035
0.03
0.025
0.02
0.015
0.01
0.005
0
0
0.05
0.1
0.15
0.2
Radius (mm)
$R(m_a^g, m_a^{g'}|r)$
Complete
Marked

b)

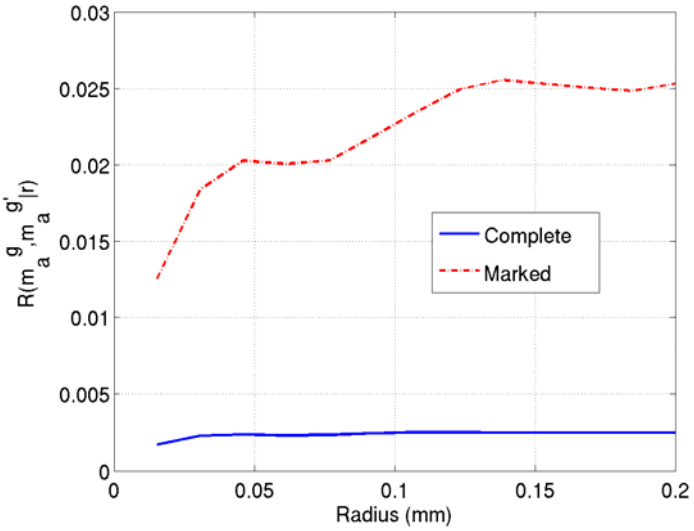

c)

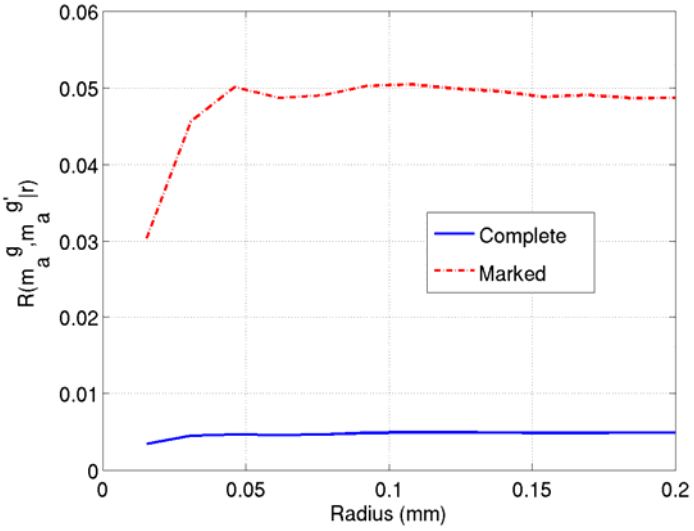

d)

Figure 14: Radial correlation functions for the complete microstructure compared with extreme value marked radial correlation functions describing the correlation between Schmid factors m_a for basal slip between 0.45 and 0.5 for the primary α phase and the Schmid factors m_a' for: a) basal slip between 0.45 and 0.5, b) prismatic slip between 0.45 and 0.5, c) pyramidal $\langle a \rangle$ slip between 0.45 and 0.5, and d) pyramidal $\langle a+c \rangle$ slip between 0.45 and 0.5 for the primary α phase in Microstructure A.

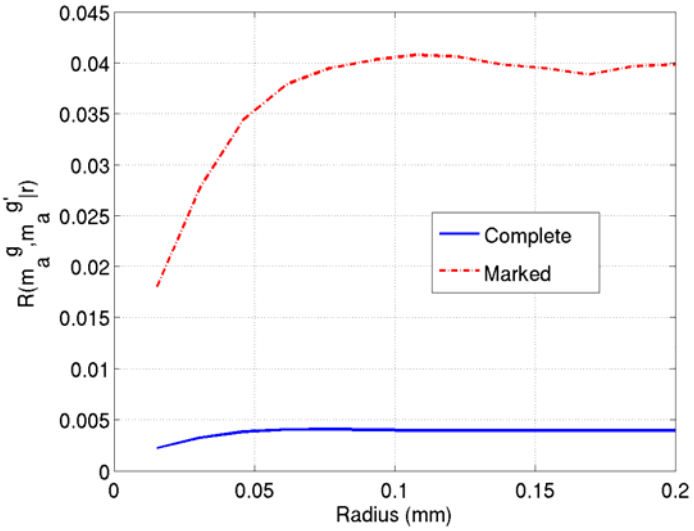
0.045
0.04
0.035
0.03
0.025
0.02
0.015
0.01
0.005
0
0
0.05
0.1
0.15
0.2
Radius (mm)
R(m_a^g,m_a^g'|r)
Complete
Marked

a)

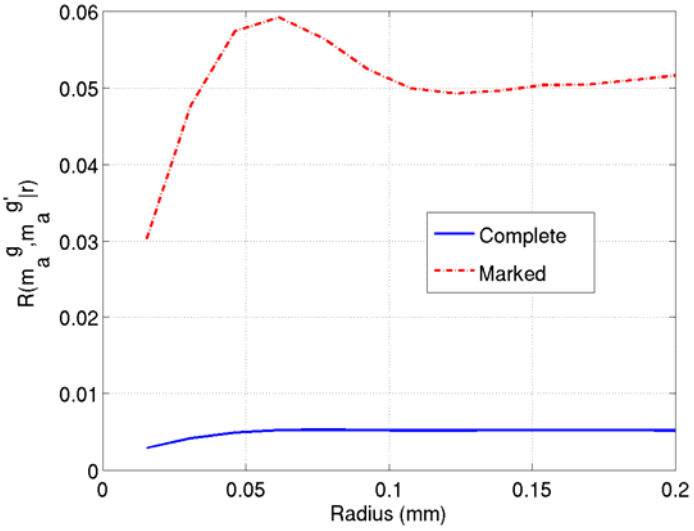
0.06
0.05
0.04
0.03
0.02
0.01
0
0
0.05
0.1
0.15
0.2
Radius (mm)
R(m_a^g,m_a^g'|r)
Complete
Marked

b)

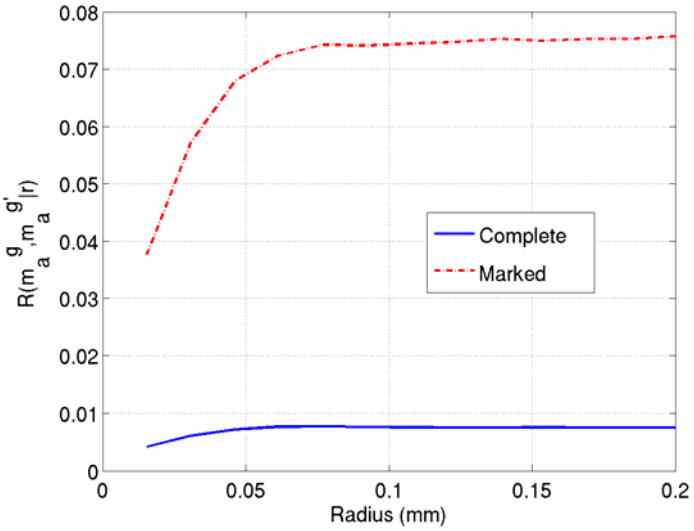

c)

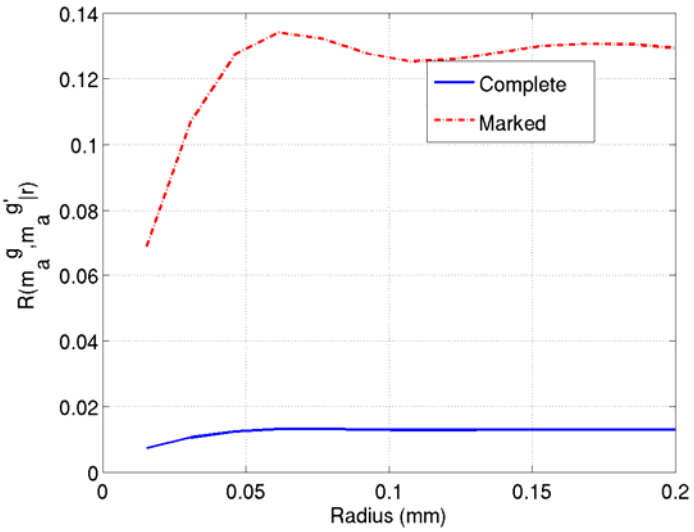

d)

Figure 15 Radial correlation functions for the complete microstructure compared with extreme value marked radial correlation functions describing the correlation between the apparent Schmid factors m_a for basal slip between 0.45 and 0.5 for the primary α phase and the apparent Schmid factors m_a' for: a) basal slip between 0.45 and 0.5, b) prismatic slip between 0.45 and 0.5, c) pyramidal $\langle a \rangle$ slip between 0.45 and 0.5, and d) $\langle 111 \rangle \{110\}$ bcc slip (transformed into the hexagonal coordinate system via the BOR) between 0.45 and 0.5 for the α+β colony phase in Microstructure A.

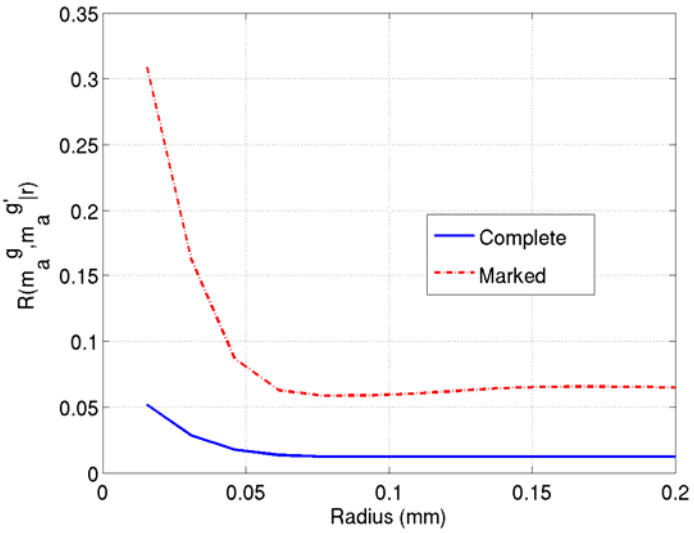

a)

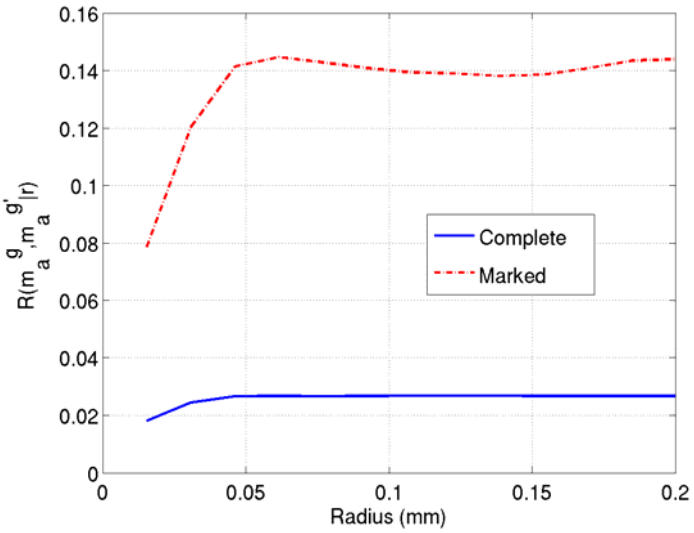

b)

Figure 16 Radial correlation functions for the complete microstructure compared with extreme value marked radial correlation functions describing the correlation between the apparent Schmid factors m_a for basal slip between 0.45 and 0.5 for the primary α phase and the apparent Schmid factors m_a' for: a) basal slip between 0.45 and 0.5 and b) pyramidal $\langle a+c \rangle$ slip between 0.45 and 0.5 for the primary α phase in Microstructure B.

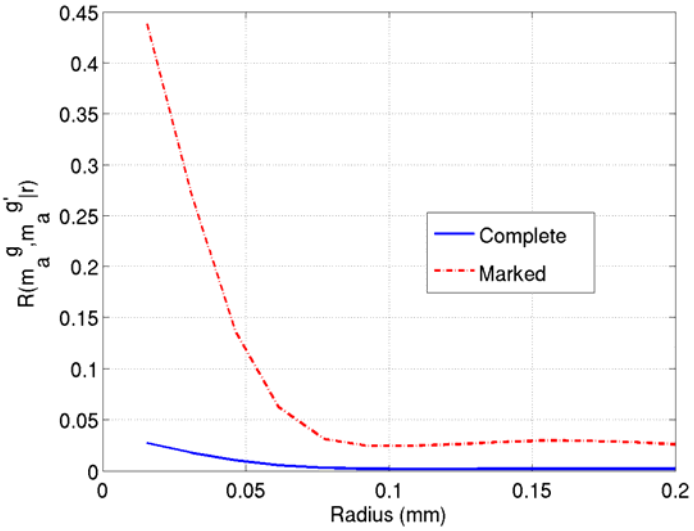

a)

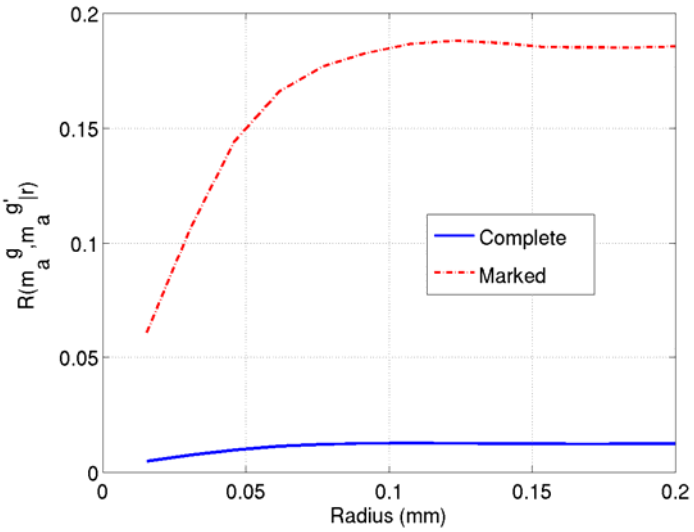

b)

Figure 17 Radial correlation functions for the complete microstructure compared with extreme value marked radial correlation functions describing the correlation between the apparent Schmid factors m_a for basal slip between 0.45 and 0.5 for the primary α phase and the apparent Schmid factors m_a' for: a) basal slip between 0.45 and 0.5 and b) $\langle 111 \rangle \{110\}$ bcc slip (transformed into the hexagonal coordinate system via the BOR) between 0.45 and 0.5 for the α+β colony phase in Microstructure C.

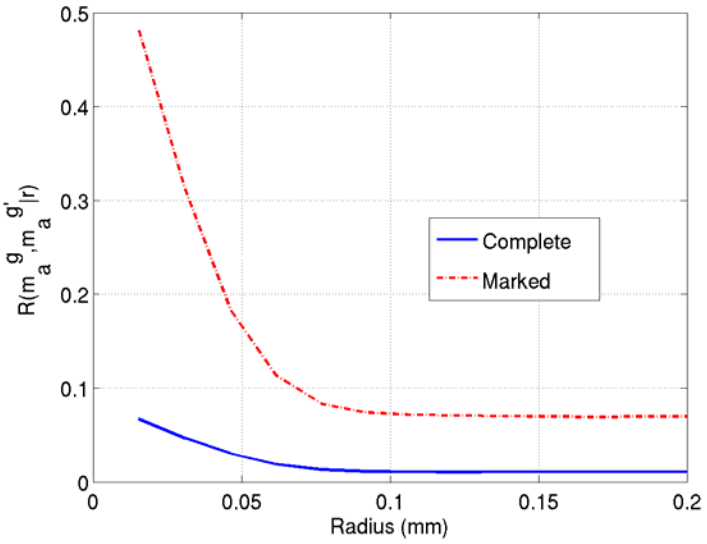

a)

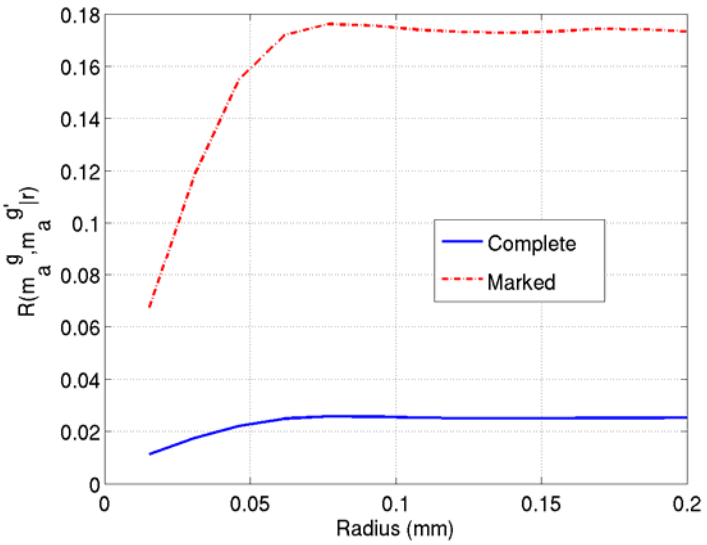

b)

Figure 18 Radial correlation functions for the complete microstructure compared with extreme value marked radial correlation functions describing the correlation between the apparent Schmid factors m_a for basal slip between 0.45 and 0.5 for the primary α phase and the apparent Schmid factors m_a' for: a) basal slip between 0.45 and 0.5 and c) pyramidal $\langle a+c \rangle$ slip between 0.45 and 0.5 for the primary α phase in Microstructure D.